Received: 23 August 2022 | Revised: 24 April 2023 | Accepted: 23 June 2023

DOI: 10.1002/suco.202200815

ARTICLE

fib CEB-FIP WILEY

Experimental and theoretical analysis of cracking and tension stiffening in UHPFRC under high-cycle fatigue

B. D. G. Sepulveda[1] | **P. Visintin**[1] | **A. B. Sturm**[2] | **D. J. Oehlers**[1]

[1]School of Civil, Environmental and Mining Engineering, The University of Adelaide, Adelaide, South Australia, Australia

[2]National Cheng Kung University, Tainan, Taiwan

Correspondence
B. D. G. Sepulveda, School of Civil, Environmental and Mining Engineering, The University of Adelaide, Adelaide, South Australia 5005, Australia.
Email: phillip.visintin@adelaide.edu.au

Funding information
Australian Research Council, Grant/Award Number: 190102650

Abstract

Tension-stiffening controls the serviceability behavior of concrete structures as it is responsible for crack formation and, consequently, the deflection of beams. In fiber reinforced concrete, such as ultra-high performance fiber reinforced concrete (UHPFRC), fibers bridge cracks and thereby transfer tensile stresses across the cracked region, allowing for tensile stresses to be carried by the concrete within the cracked region. Due to structures being designed for longer design lives, the consideration of long-term effects such as fatigue is required. Much research has examined tension-stiffening under fatigue when subjected to low cyclic loading, but very little has considered the effects of high-cycle fatigue, especially for UHPFRC. This paper presents the results of nine UHPFRC tension-stiffening tests under high-cycle fatigue in which the crack formation and development under varying cyclic ranges were studied. Specimens were subjected to as many as 5.7 million cycles, and crack readings were taken during each test. The experimental results demonstrate the random nature of cracking on UHPFRC as well as the increase in the crack width under cyclic loads. Finally, this research described the extension of an existing partial-interaction mechanics model to allow for the stress in the fibers and the increase in crack width due to high cycle fatigue.

KEYWORDS

crack evolution, high-cycle fatigue, partial-interaction, tension-stiffening, UHPFRC

1 | INTRODUCTION

Tension-stiffening of reinforcement embedded in concrete has a significant impact on serviceability design because the composite action that arises due to bond between the reinforcement and the surrounding concrete stiffens the response of the reinforcement in cracked regions and restrains crack opening. The importance of tension-stiffening in controlling member deflection and crack-widths is well recognized. Extensive testing has allowed for the development and validation of models that can predict tension-stiffening and concrete cracking behavior: under instantaneous[1–3] and sustained loads[4,5]; that can further allow for alternative concretes such as those which contain fibers[6,7]; or alternative reinforcement such as those manufactured from fiber reinforced polymer.[8]

Despite the importance of tension-stiffening both in initial design and in controlling the service life (by limiting crack width leading to an improvement in durability), very little research has focused on the impact of high-cycle

fatigue on tension-stiffening.[9,10] Furthermore, design standards such as the Eurocode 2 and AS3600:2018[11] do not consider the effect of the fatigue on tension-stiffening behavior.[12,13]

Many studies have focused on experimentally quantifying the impact of high-cycle fatigue on the material properties that control tension-stiffening, that is, the stress/strain behavior of the reinforcement (σ_r/ϵ_r) and concrete (σ_c/ϵ_c) and the bond stress/slip relationship between the reinforcement and concrete (τ/δ).[14–23] However, relatively little testing has been conducted at the mechanism level. For example, few previous studies have tested reinforced concrete tension elements under high cycle fatigue to observe average strains over the element, local strains at cracks and crack-widths.[10,24]

When considering the development of analytical models, there is again very little work devoted specifically to the study of tension-stiffening under high cycle fatigue. Fantilli and Vallini[25] developed a one-dimensional finite element model using a fictitious crack approach to allow for concrete in tension and a bond/slip (τ/δ) relationship with a negative shear stress component to allow for damage to the bond during unloading. Zanuy et al.[9] developed a modified τ/δ relationship to allow for damage during high-cycle fatigue and applied this material model using an analytical partial-interaction approach based on the work of Tassios and Yannopoutos[26] to predict tension-stiffening and crack widening in an element with an already stable crack pattern. This work was later extended to allow for the additional impact of concrete shrinkage by Zanuy et al.[27] Visintin et al.[28] and Shukri et al.[29] developed detailed partial-interaction models that simulate the formation and widening of cracks and tension-stiffening under cyclic loads using a numerical partial-interaction model that allows for non-linearity in σ_r/ϵ_r and τ/δ relationships, and that can also predict the formation of new cracks under cyclic loading. The models of Visintin et al.[28] and Shukri et al.[29] were further incorporated into member models and showed that the cyclic behavior of a member under flexure is highly dependent on the impact of tension-stiffening.

Ultra-high performance fiber-reinforced concrete (UHPFRC) is a relatively new cementitious composite that is characterized by high compressive strengths, strain-hardening in tension, significant post-cracking tensile strength and very high durability. These material properties make UHPFRC ideal for application in structures such as bridges where long-service lives and low maintenance requirements are desirable.[30–33] Although ideal for application in bridge structures, relatively little work has been focused on quantifying fatigue material properties for concrete in compression[34–36] or tension,[37,38] or to understand the impact of high-cycle fatigue on bond properties.[39] Because associated fatigue material properties have not been widely reported, there are significant challenges in using these results to validate analysis and design approaches.

Most flexural experimental test performed with UHPFRC beams were at material level, without reinforcement.[40–45] At the member level there is limited design guidance to deal with reinforced UHPFRC under high cycle fatigue and limited number of experimental test of reinforced UHPFRC reported. For example, Sawicki and Brühwiler[46] show the results of three different T cross-section full scale beams under high cycle fatigue with the longest experimental campaign, in which one specimen was subjected to almost 27 million cycles. Although this work at the member level is important to understand the overall member behavior under fatigue, it is difficult to isolate the impacts of fatigue on the tension stiffening mechanism from a flexural test and this understanding is required to develop new design guidelines.

To address this limitation and to allow for the development and validation of approaches to predict tension-stiffening and crack opening under high-cycle fatigue, in this paper, the results of a series of high-cycle fatigue tests on UHPFRC tension prisms are reported. These prisms are constructed using a UHPFRC mix design that has previously been investigated at the material level to identify the impact of high-cycle fatigue on direct tension[18] and bond τ/δ[19] behavior such that the results at the mechanism level can be related to the underlying material properties. Having presented results showing the impact of high-cycle fatigue on tension-stiffening and crack-widths, a detailed partial-interaction approach for simulating the tension-stiffening and cracking behavior is described and its application to UHPFRC is validated. Having developed and validated the numerical model, it is used as the basis for a simple parametric study to show sensitivity to reinforcement ratio and concrete shrinkage and creep.

2 | EXPERIMENTAL PROGRAM

To investigate the impact of high-cycle fatigue on the tension-stiffening behavior of UHPFRC, nine tension stiffening prisms were tested, of which seven were subjected to high-cycle fatigue, and two were subjected to monotonic loading to act as control specimens.

2.1 | Specimens, test rig and instrumentation

A tension-stiffening specimen used in the experimental program is shown in Figure 1a with a corresponding

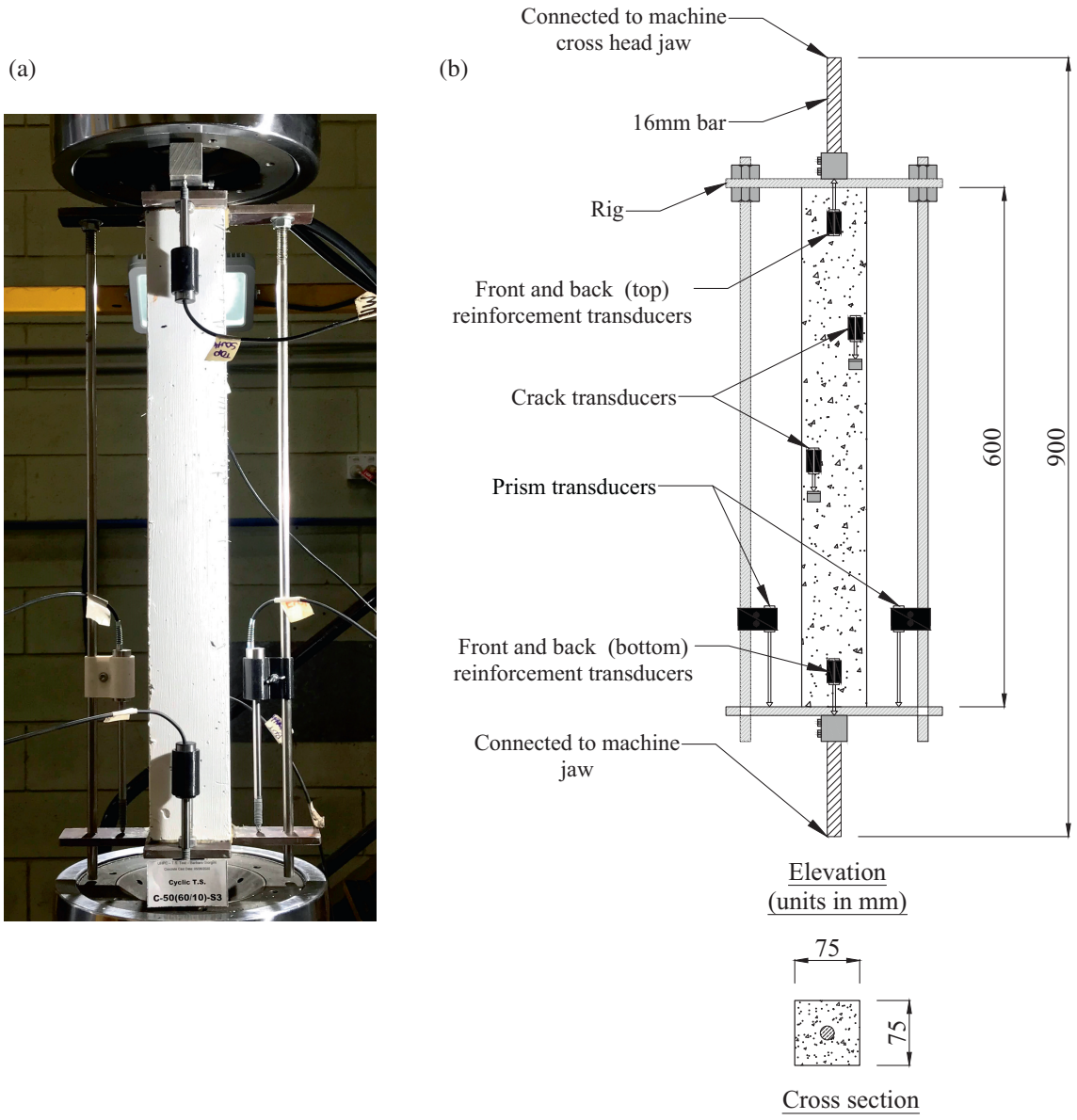

FIGURE 1 Tension stiffening test set up: (a) Specimen set up and (b) elevation and cross-section.

schematic, including the test set-up and instrumentation in Figure 1b. The test region of the specimens consists of a 75 × 75 × 600 mm UHPFRC concrete section which is reinforced with a single 16 mm diameter ribbed steel bar that passes through the centroid of the cross-section. The bar extends 150 mm beyond the concrete at each end of the test specimen to allow it to be gripped by the jaws of a universal testing machine.

As shown in Figure 1, a steel rig, identical to that used by the authors in previous studies on the monotonic tension-stiffening behavior,[47] was epoxied to the top and bottom face of the prism to allow for the attachment of the instrumentation. To allow for the measurement of the total elongation of the prism, two LVDTs with 25 mm gauge lengths were attached to bars extending along the entire prism length, and two 20 mm LVDTs were located at each end of the specimen to measure the slip of the reinforcement relative to each concrete face.

To allow for interpretation of the tension-stiffening and crack-width test results, additional tests were conducted to assess the material properties of the UHPFRC and steel reinforcement. To quantify the concrete fiber tensile stress/strain (σ_c/ϵ_c) and fiber stress-crack width (σ_c/w) behavior, nine prismatic specimens with a 100 × 100 mm cross-section and a 300 mm length were produced as in Figure 2a. These specimens were then notched at the mid-height to have a 75 mm × 75 mm test region to mirror the dimensions of the tension stiffening prism. To allow the concrete to be loaded in direct tension, 16 mm reinforcing bars were embedded 100 mm

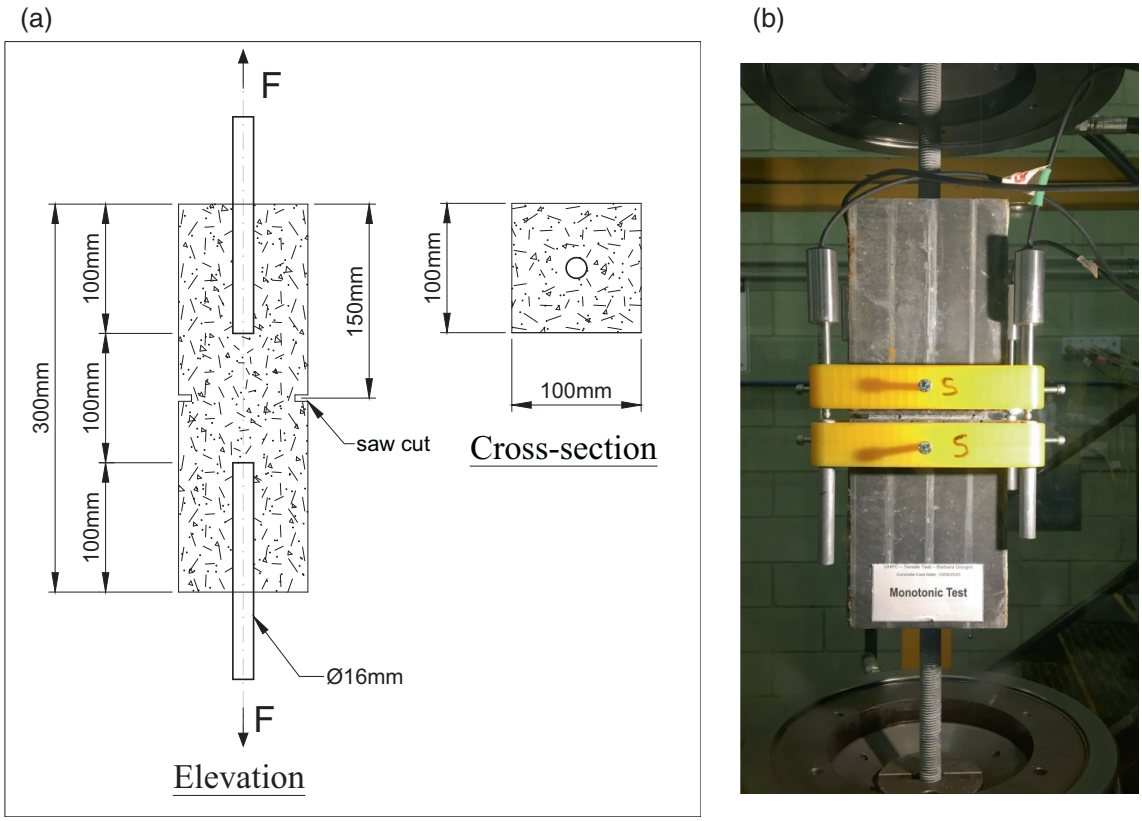

FIGURE 2 Tensile test specimen.

into each end of the concrete such that the central 100 mm of the specimen remained unreinforced, as in Figure 2a. Given that the test region was located more than 3.5 times the fiber length (13 mm) from the tip of the reinforcing bar, the presence of the reinforcement does not impact the stress-crack width behavior along the notch, and the results are compatible with those from dogbone shaped prisms.[18]

During testing, as shown in Figure 2b, the reinforcing at each end of the specimen was gripped in the jaws of a universal testing machine, and a load was applied at a displacement rate of 0.1 mm/min until a notch opening of 0.4 mm was recorded; afterwards, the rate was changed to 0.4 mm/min until the load had reduced to virtually zero. Throughout testing, the width of the crack that formed through the notch was measured at the four corners using 25 mm LVDTs. This test procedure was developed previously for the tension analysis of a cracked UHPFRC under fatigue and further details about the test can be found in.[18]

To quantify the concrete compressive strength, 23 standard cylindrical prisms with a diameter of 100 mm and a height of 200 mm were produced. Specimens were tested in triplicates throughout the period over which the tension stiffening tests were conducted to monitor for any change in concrete strength and elastic modulus. Specimens were tested under uniaxial compressive loads at a load rate of 1.148 kN/min in accordance with AS 1012.17:1997[48] and the peak load recorded.

TABLE 1 UHPFRC mix design.

Material	Mix ratio (by mass)	Mix (kg/m^3)
Cement	1	960
Sand	1	960
Silica Fume	0.266	255
Water	0.190	182
Superplasticiser	0.045	43
Steel Fibre (2% concrete vol.)	0.164	157

Four prisms with a cross-section of 50 mm × 50 mm and a length of 285 mm were used to measure total concrete shrinkage strains in accordance with ASTM:C157/C157M-08.[49] The shrinkage specimens were demolded at the same time as the test specimens and stored in identical conditions throughout the curing and testing period. The zero-time at which the initial length of each prism was recorded was at the time of demolding, which was 48 h from casting.

The stress–strain relationship of the 16 mm reinforcing bar was measured in accordance with ISO 6892-1[50] to obtain the elastic modulus and yield strength.

TABLE 2 Monotonic test.

Specimen	Age (days)	f_c (MPa)
M1	238	147
M2	344	147

2.2 | Materials and specimen preparation

All test specimens were cast from a single batch of concrete that was prepared using the UHPFRC mix design in Table 1, which is identical to that used by the authors to quantify the high-cycle fatigue properties under uniaxial tension[18] and the high-cycle fatigue bond resistance between UHPFRC and 16 mm reinforcing bars.[19] The mix design consists of a sulfate-resisting cement (Type SR) conforming to the requirements of AS 3972:2010,[51] from Adbri Adelaide Brighton Cement, a densified amorphous silica fume conforming to the requirements of AS/NZS3582.3:2002,[52] brand ECOTEC, a mined double-washed sand and a high-range water reducing agent with retarder (Sika ViscoCrete10). The high-strength steel microfibers were the DAYE WSF Micro Steel Fibre, from Daye Fibre, which were incorporated into the mix design have a diameter of 0.2 mm, a length of 13 mm and a yield strength of 2850 MPa. The w/c ratio used is 0.19 as specified in Table 1.

To prepare the concrete, all the dry ingredients were added to a planetary mixer with a maximum capacity of 0.5 m^3. The mixer was run for 5 min, at which point the dry materials were visibly blended. The water and water reducing agent were then slowly added, and mixing continued until the concrete was visibly flowable (approximately 20 min). Finally, the fibers were added, and the concrete was mixed for a further 5 min to ensure good dispersion.

Following mixing, all specimens were cast and finished before being covered with wet hessian and plastic in ambient lab conditions for 2 days. After 2 days, all specimens were demolded and stored in ambient lab conditions until the time of testing.

2.3 | Tension stiffening test procedure

2.3.1 | Monotonic tests

Two tension stiffening tests, designated M1 and M2 in Table 2, were conducted under monotonic test conditions; one at the beginning of the experimental test campaign (238 days after casting) and one at the end of the fatigue testing campaign (344 days after casting).

During the monotonic tests, each specimen was loaded under displacement control at a rate of 0.6 mm/min until the first crack was observed (indicated by a change in slope of the load elongation relationship as previously observed by Visintin et al.[47]). In Figure 3 the load vs. time chart schematically illustrates the monotonic test represented by the dashed line O-A-B-C-D-E-F-G-H-I-J. After the first crack formed point A in Figure 3, the test was paused, and the displacement was held while the cracks on opposite faces of the specimens were marked, and the crack widths were measured using an optical microscope with a 0.001 mm precision. The crack width readings are represented in Figure 3 by the dots. The load was then increased at the same 0.6 mm/min displacement rate with pauses at each 10 kN increment to mark the formation of new cracks and to measure crack widths at points B-C-D-E-F-G-H in Figure 3. The final set of crack width readings was taken at 90 kN (point H in Figure 3) of the applied load. The specimens were then loaded till the yield of the reinforcement at a peak of 110 kN (point I in Figure 3), after which they were unloaded (point J in Figure 3).

2.3.2 | Cyclic tests

In Figure 3, the cyclic test is presented through a load vs. time chart given by the continuous line O-A-B-C-D-E-K-L-J-M-N-Q-S-T-U-V-X-Z. To perform a cyclic test, the specimens were loaded at 0.6 mm/min until the first crack formed (identified by a change in slope of the load–deflection relationship and represented schematically by the at point A in Figure 3). The location of the cracks was then marked, and their width measured using the optical microscope. Specimens were then loaded in the same way as the monotonic specimens, taking measurements of crack spacing and crack width at 10 kN increments until the target peak load was reached as shown in Figure 3. Once the peak load was reached (point E, in Figure 3), the specimens were unloaded to the trough load (point K) at 0.6 mm/min, and the crack widths were recorded. Finally, the specimens were reloaded to the mean cyclic force (point L) and then cycled through the specified load range at a frequency of 10 Hz.

Crack width readings at the trough (T) and peak (P) of cyclic loadings were then taken after 865,000 cycles (which is equivalent to one full day of cyclic loadings) represented in Figure 3 by points M and N respectively. Daily readings were then recorded until the test reached more than 5 million cycles were achieved, where the tests were considered to have run-out (named loaded to failure (LF) tests) or until the failure under fatigue loading had

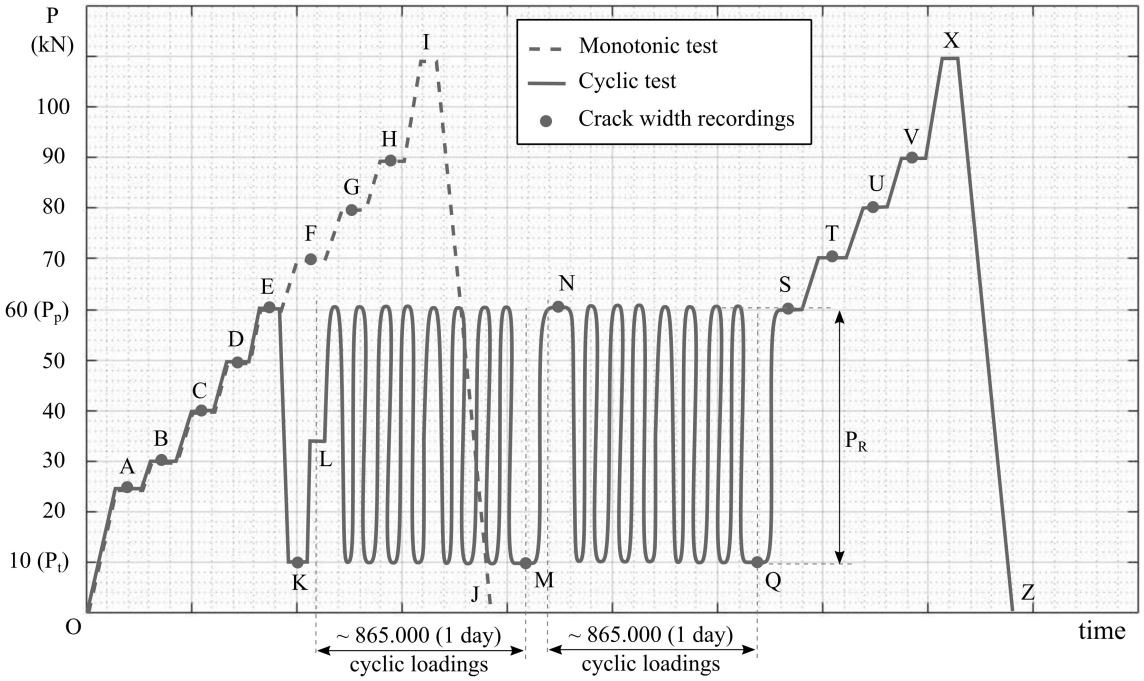

FIGURE 3 Schematic representation of test procedure over time.

occurred. In the case of LF tests, after reaching 5 million cycles, the test was paused to measure the cracks at the trough (point Q in Figure 3) and peak (point S in Figure 3). To finish the test, the specimen was again loaded in a rate of 0.6 mm/min with pauses at each 10kN load step as represented by points T, U, V in Figure 3 while measurements of crack width were taken. The last crack measurements were taken at 90 kN and finally the specimen was loaded up to 110 kN (point X) before be unloaded to 0 kN (point Z).

As an example of the procedure, for a 50% range (R) test, where R is the difference in load between P and T, all the steps were performed for the case of a LF test with a peak load (P_p) of 60 kN and trough load (P_t) of 10 kN. Starting at point O (Figure 3), the specimen is loaded until the first crack forms, given by point A at a load of 25 kN in Figure 3. Cracks are marked and recorded with the microscope. Afterwards, the machine is loaded until a load of 30 kN is obtained as shown by point B in Figure 3, where the cracks are again measured. In steps of 10 kN (points C, D, E in Figure 3) this procedure is repeated. Once the target peak load P_p of 60 kN is reached (point E Figure 3), cracks are again measured and then the specimen is unloaded to the trough load P_t of 10 kN (point K), where again the crack widths are recorded.

To allow for the continual measurement of the width for selected cracks throughout testing, prior to the commencement of cyclic loading, up to three 5 mm LVDTs were glued to the concrete surface to measure the growth of the three largest cracks identified during the monotonic component of the load history (see Figure 1b). To identify any new cracks which formed during cyclic loading, and to obtain detailed measurements of all crack widths after each 24-h test period, the loading was paused at the peak and trough to measure crack spacing and crack width.

Before commencing the cyclic portion of the test, the specimen is loaded up to the mean cyclic load which is in this case is 35 kN (point L) so that the sinusoidal cyclic loading can commence reaching the peak of 60 kN and a trough of 10 kN. Readings at 10 kN (point M) and 60 kN (point N) are taken daily repeating the procedure until 5 million cycles is reached where the readings at 60 kN (point Q) and 10 kN (point S) are again recorded before the test is monotonically loaded to failure as per the S-T-U-V-X-Z curve in Figure 3.

TABLE 3 Cyclic test.

Specimen	Age (days)	P_P (kN)	P_T (kN)	P_R (kN)
C1	251	28.29	10.91	17.39
C2	264	28.37	10.84	17.52
C3	336	29.93	10.03	19.90
C4	249	55.75	13.67	42.08
C5	259	55.38	14.23	41.15
C6	258	81.07	19.22	61.85
C7	273	81.37	18.64	62.74

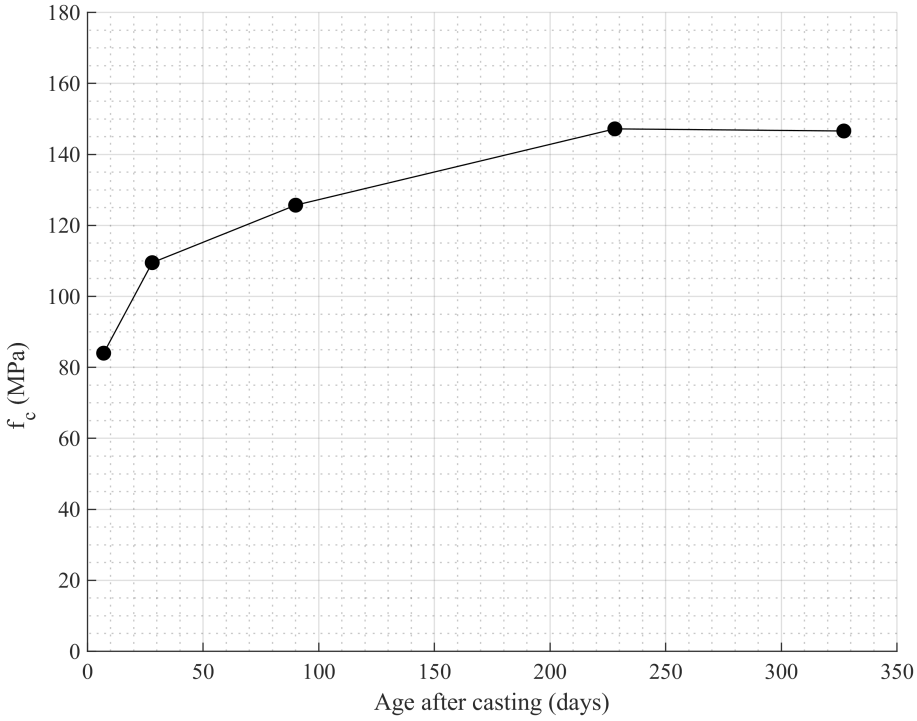

FIGURE 4 Average concrete strength development during time.

Details of the seven tension stiffening tests conducted under cyclic loading are provided in Table 3. The specimens were designated C1–C7 and were all tested between 251 and 336 days after concrete batching.

3 | RESULTS AND DISCUSSIONS

3.1 | Material properties

The change in concrete compressive strength (f_c) measured throughout the 336-day period from casting to testing is shown in Figure 4, where each point represents the average of three tests. The results show that by the time that tension-stiffening tests commenced at day 230 the compressive strength remained essentially constant at 147 MPa.

The results of the concrete direct-tension tests are shown in Figure 5, where the load is plotted against the crack-width measured across the notch. Three direct tensile tests were undertaken at 230, 331 and 421 days, and the average result at each concrete age is shown in Figure 5a. Given that the concrete strength did not change significantly over the test period, in addition to the average results at each concrete age, the average of all test results is also provided.

In Figure 5b, the results obtained from monotonic dogbone testing of specimens with a cross-section of 120 mm × 120 mm and a shank length of 300 mm but cast from a different batch of concrete with the same mix design. Full details on the test specimen design and testing procedure can be found in.[18] As expected, these dogbone test results show very similar post-cracking σ_c/w behavior, particularly when considering the difference in concrete age (dogbones tested between 140 and 153 days). It is therefore suggested that the dogbone results can be used as the basis for modeling the strain-hardening behavior of this particular UHPFRC mix design. In Figure 5c, the σ_c/w is converted to an equivalent σ_c/ϵ by taking a gauge length of 300 mm.

The concrete shrinkage strain measured relative to a 48-h zero-time is shown in Figure 6 where it can be observed that shrinkage increases at a relatively rapid rate until approximately 250 days after the zero time. After this point, the concrete shrinkage strain remains relatively constant at an average of approximately 600 με.

The reinforcement σ_r/ϵ_r relationship is shown in Figure 7. From this relationship, the 0.2% proof stress was calculated to be 535 MPa and the elastic modulus 203 GPa.

3.2 | Tension-stiffening

3.2.1 | Monotonic tension stiffening

The results of the monotonic tension-stiffening tests are shown in terms of the measured load average strain (P/ϵ_{avg}) relationship in Figure 8a, where the average strain is calculated using the average deformation measured by

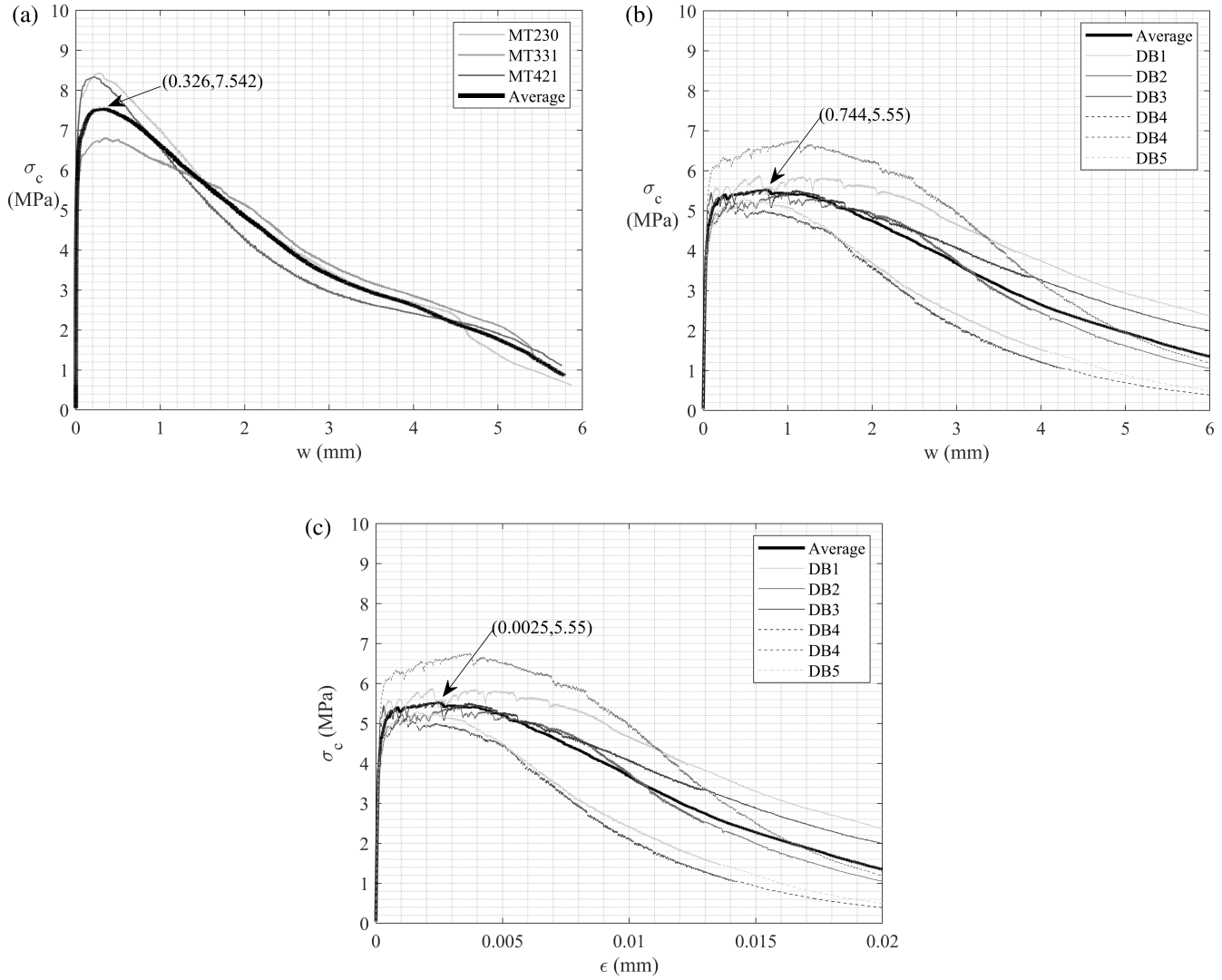

FIGURE 5 (a) Concrete tensile response obtained from notched prisms, and (b) σ_c/w and (c) σ_c/ϵ_c obtained from dogbone testing (reproduced from Sepulveda et al.[18]).

the 2 LVDTs that measure total specimen elongation (Figure 1) divided by the specimen length (600 mm). The results in Figure 8a are used to quantify the tension-stiffening stress σ_{ts} in Figure 8b, which is calculated by subtracting the force that would be developed in a bare bar (P_{bb}) from the measured force in the tension stiffening prism (P) at each measured average strain, and converting the difference between these forces to a stress by dividing by the area of the concrete (A_c), as given by Equation (1). Importantly, while giving a general indication of the gross amount of tension stiffening, this approach does not capture the variation in stress of the reinforcement and the concrete that occurs between cracks.

$$\sigma_{ts} = \frac{P - P_{bb}}{A_c} \quad (1)$$

The results in Figure 8 show that despite more than 100 days between testing of the two specimens, very consistent magnitudes of tension-stiffening are obtained, and this is because the concrete shrinkage strains had largely stabilized by the time of testing (Figure 6). The results are characterized by the onset of cracking at 26 kN for specimen M1 and 24 kN for specimen M2 and then relatively stable tension-stiffening up until 60 kN (55% of the yield force), beyond this point the tension-stiffening stress begins to rapidly reduce (shown by the reduction in σ_{ts} for average strains greater than 0.001).

3.2.2 | Cyclic tension stiffening

In Table 4, the load range P_R, peak load P_p, trough load P_T and are normalized by the yield force P_y and shown as

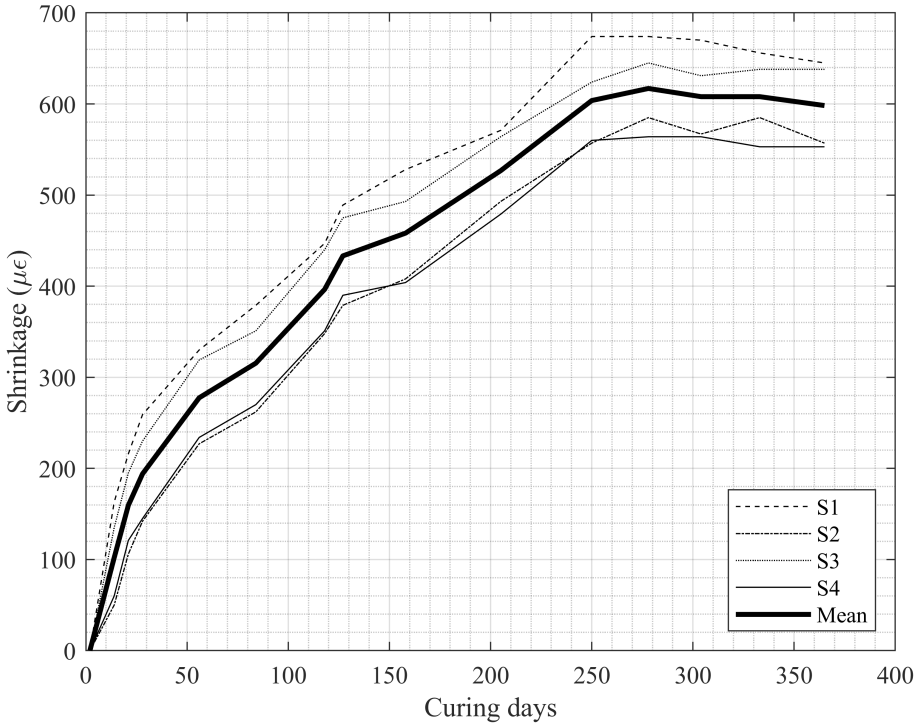

FIGURE 6 Concrete shrinkage during time.

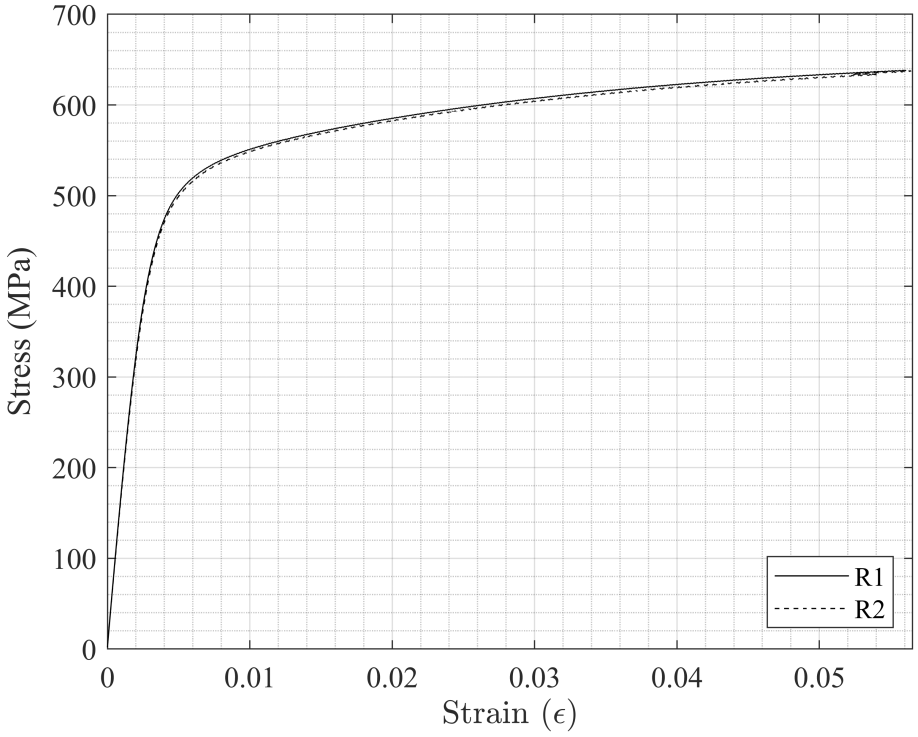

FIGURE 7 Reinforcement stress–strain curve.

the range R, peak P and trough T. Also shown in Table 4 is the number of cycles each specimen was subjected to prior to either loading to failure (LF), or the reinforcement fatigue fracture (RFF) outside of the concrete test region. The specimens were loaded at cyclic load ranges (P_R) of between 16.2% and 58.6% of the reinforcement yield force (P_y), which was measured to be 107.2 kN. The peak loads (P_P) ranged between 26.4% and 75.9% of the yield force (P_y). The trough loads (P_T) ranged between 9.4% and 17.9% of the yield force (P_y). Also, the P/ϵ_{avg} and $\sigma_{ts}/\epsilon_{avg}$ results of the seven cyclic tests are shown in Figure 9 along with the results of the monotonic test which acts as a control to help identify changes in behavior due to fatigue.

By comparing the result of the cyclic and monotonic tests with different peaks and ranges in Figure 9, it can be seen that regardless of the magnitude of cyclic range, an increase in specimen average strain occurs. The increase in the average strain under cyclic loading is shown in Figure 10. The increase in average strain in Figure 10 is observed to be initially rapid before stabilizing to be virtually constant increase, even in cases where the specimen was cycled to failure (specimens C4–C7). Importantly, it can also be seen in both the load–average strain responses and the tension stiffening stress–average strain responses in Figure 9, that although the average strain may increase due to cyclic loading, provided that the specimen does not fail, if later loaded monotonically after a period of cycling, the tension stiffening response is similar to that obtained under monotonic loading. That is, the monotonic response provides an envelope to the high-cycle fatigue response.

From Figure 10, it is observed that there is an initial period in which the average strain increases relatively rapidly with a small number of cycles before the response enters a second stage in which there is stable increase in average strain with N. Furthermore, in Specimens C4 and C5 where the specimens fail under cyclic loading, there appears to be a small increase in average strain just prior to failure. This general behavior mirrors the increase in slip per cycle observed for UHPFRC tensile stress crack width and bond stress slip measured by Refs. 18,19.

As an example of the magnitude of increase of average strain, consider specimens C1 and C6 as an example. These specimens have a range of 16% and 58% of the yield stress, respectively (Table 4). An increase in average strain is observed in both specimens, with C1 starting at 0.00024 and finishing at 0.0003 after 5,000,125 cycles (Table 4). Specimen C6, had an average strain at the beginning of cyclic loading of 0.00152 and after 134,491 cycles, the average strain increased to 0.00171. This demonstrates the influence of cyclic range on the rate of increase of the average strain. The same general behavior is observed for specimens C4 and C5 with 39% and 38% range, respectively.

Specimens C1–C3 in Figure 9 were subjected to cyclic stresses with a range of approximately 16% of P_y and, as shown in Table 4. These specimens did not fail after being subjected to between 4.8 and 5.7 million cycles. Given the length of testing, these specimens were considered to have run-out and were therefore loaded monotonically to failure after cyclic loading. The results of these tests (loaded to failure) in Figure 10 show that despite the increase in average strain during cyclic loading, the tension stiffening stress tends to that of the monotonic tests when loaded to failure. The reason for this is that both the σ_c/w and τ/δ behaviors of the bond have been shown to approach the monotonic backbone relationship after a period of high-cycle fatigue loading.[18,19]

Specimens C4–C7 in Figure 9 failed by reinforcement rupture during cyclic loading, with the number of cycles to failure N given in Table 4. For specimens C4, C6 and C7, the test was stopped when the reinforcement outside of the test region ruptured, but in specimen C5, the

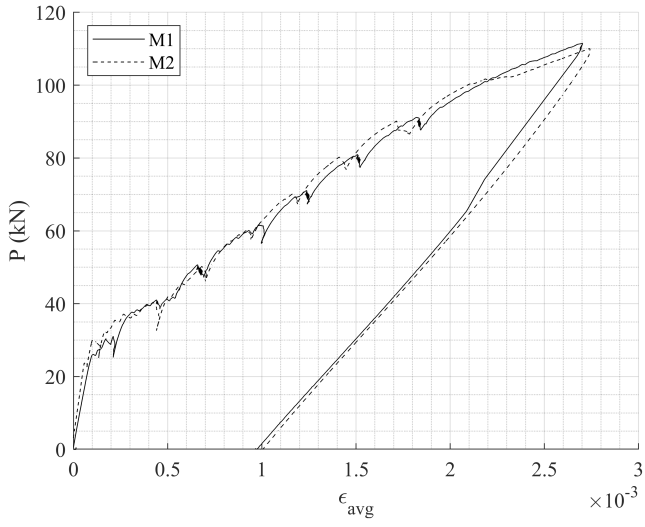

FIGURE 8 (a) Monotonic load–average strain results and (b) monotonic tension stiffening stress–average strain results.

TABLE 4 Cyclic test results.

Specimen	P (P_P/P_y)	T (P_T/P_y)	R (P_R/P_y)	Number of cycles (N)	Failure mode
C1	0.264	0.102	0.162	5,000,125	LF
C2	0.265	0.101	0.163	4,870,017	LF
C3	0.279	0.094	0.186	5,788,648	LF
C4	0.520	0.128	0.393	676,580	RFF
C5	0.517	0.133	0.384	1,120,683	RFF
C6	0.756	0.179	0.577	134,491	RFF
C7	0.759	0.174	0.585	133,040	RFF

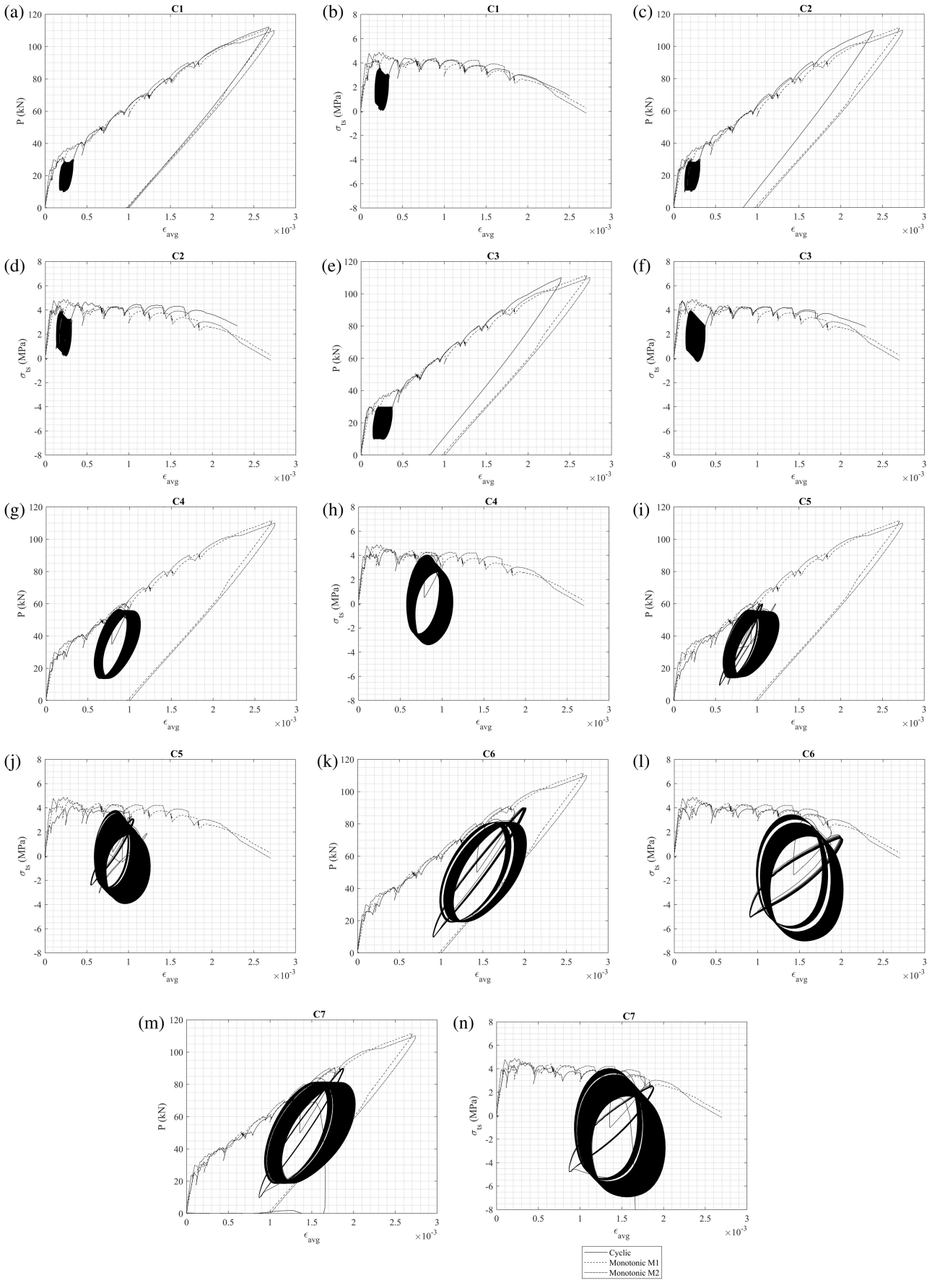

FIGURE 9 Load strain and stress strain for cyclic tension stiffening tests.

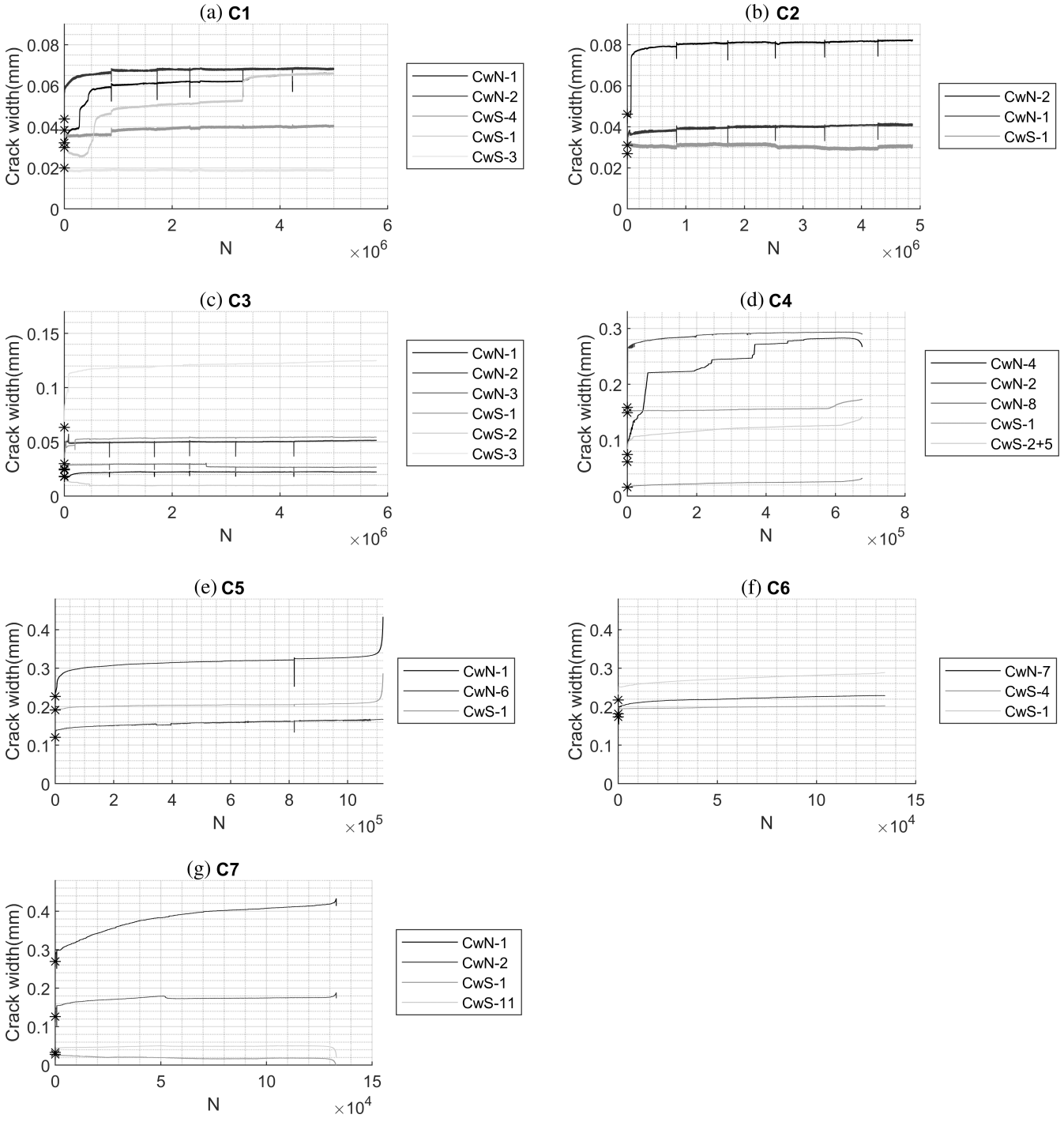

FIGURE 10 Crack widths measures during cyclic loading.

reinforcement ruptured within the concrete, ultimately causing the fibers to pull out at the location of the rupture.

In Figure 10d,e, for specimens C4 and C5, it can be seen that failure occurred once the specimen reached an average strain of approximately 0.0011, even though both tests presented a different number of cycles. That is, specimen C4 underwent 676,580 cycles before failure, while specimen C5 underwent 1,120,683 cycles. In the case of specimens C6 and C7 (Figure 10f,g), failure occurred after the specimen reached the strain of 0.002 when both specimens had reached around 133,000 cycles.

The tension-stiffening stress, given by the $\sigma_{ts}/\epsilon_{avg}$ charts in Figure 9b,d,f,h,j,m,o follow the monotonic backbone obtained for specimens M1 and M2. Figure 9b,d,f shows the tension stiffening stress behavior after cyclic loading when specimens C1, C2 and C3 were loaded to failure. For the specimens loaded to failure in Figure 9b,d,f, it can be seen that the fatigue result

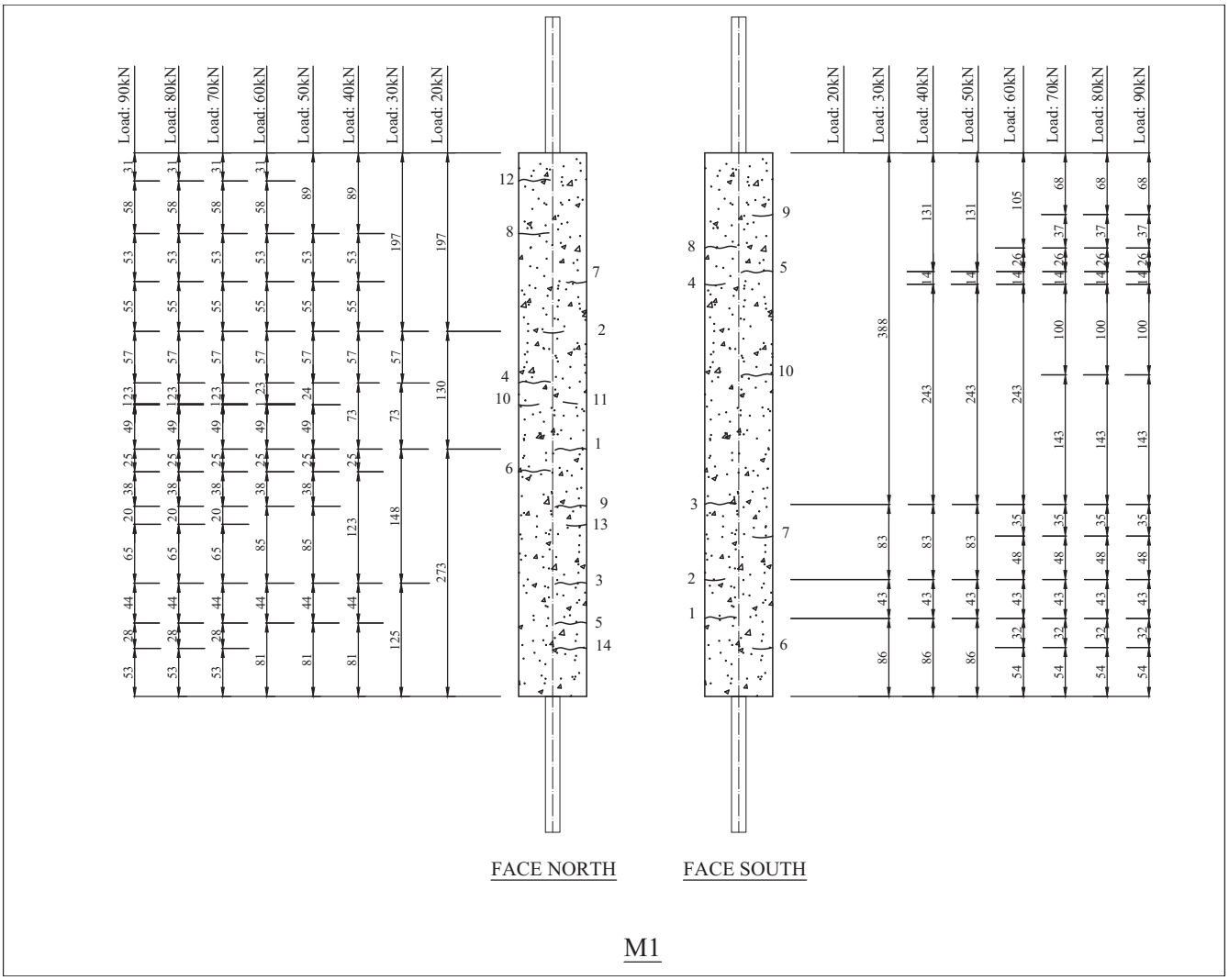

FIGURE 11 Detailed crack mapping of test specimen M1.

represented by the continuous line is not significantly affected by the previous load history. Results for specimens C4–C7 show the effect of cyclic loading only, as the specimens failed during fatigue testing.

3.3 | Crack spacing and width

3.3.1 | Monotonic loading

The location and width of each crack measured at each monotonic load step is summarized in Appendix S1, with an example of the crack mapping shown in Figure 11 for specimen M1.

The detailed mapping shows the location of each crack on opposing sides of the tension stiffening prism (identified as North and South). Of note is the random nature of the formation of the initial cracks, and that cracks did not form through the entire depth of the prism at low load levels. This behavior is likely because of local variation in both the fiber density and orientation, which provides local variations in tensile strength and material properties. As the load level increases, it can, however, be seen that the cracks rapidly stabilize and extend to both faces of the specimen. This behavior was identified to be typical of all tests, regardless of if they were loaded under monotonic or cyclic conditions.

Given the significant number of cracks, it is more meaningful to consider the variation in crack-width and crack-spacing under a given load level. To allow this, all measurements of crack-spacing and crack-width obtained during monotonic loading (both in the monotonic tests and in the cyclic tests prior to the initiation of cyclic loading) were collated. The distributions of crack spacing and crack width are shown in Figure 12. In these boxplots, the boxes indicate the range of the first and third quartile

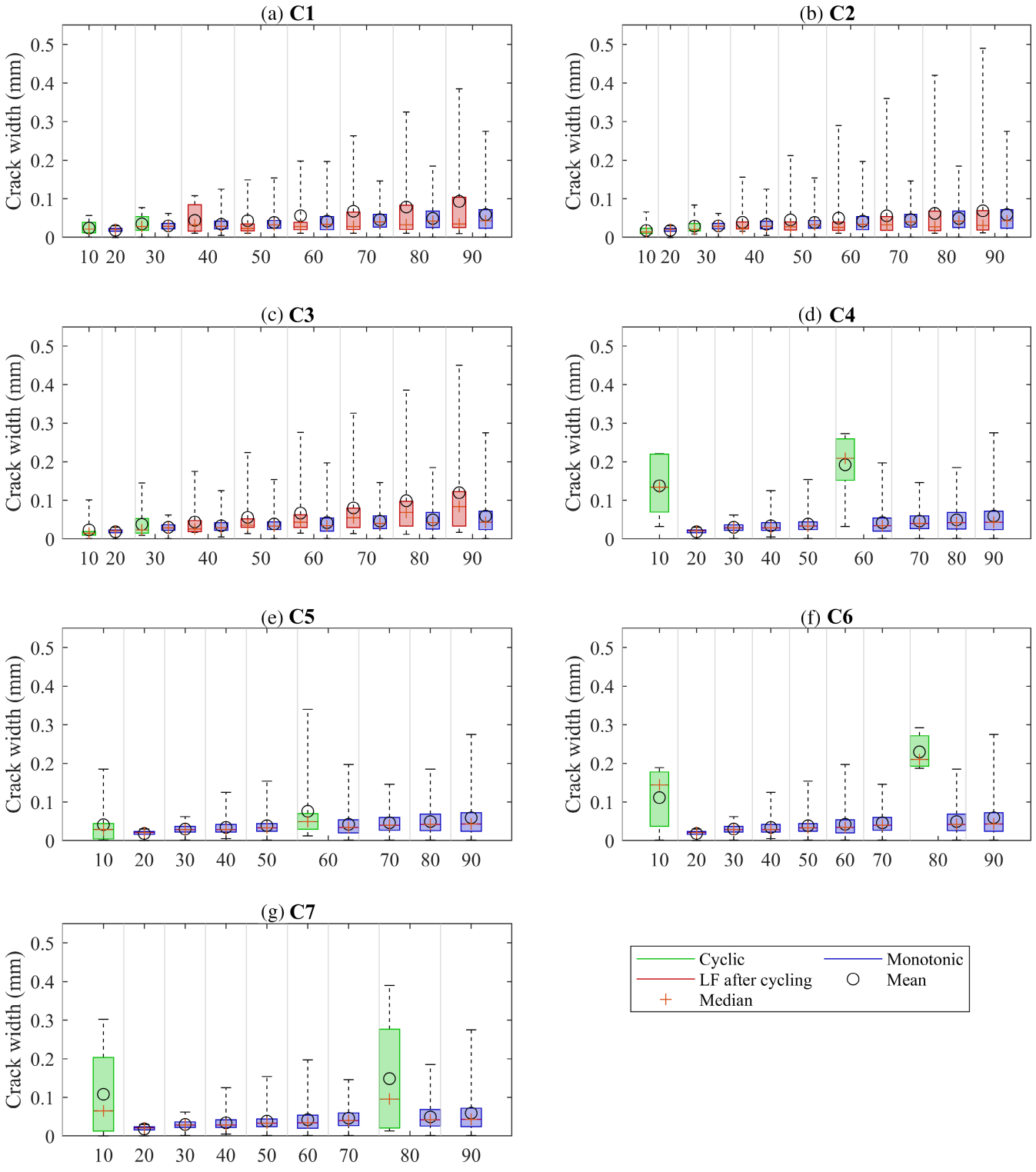

FIGURE 12 Compiled monotonic results including data from monotonic and cyclic tests before start the cyclic loading.

of all readings, the whiskers give the total range of the maximum and minimum readings, the cross within the box indicates the median, the circle marker indicates the mean reading and the number above each box plot indicates the number of experimental observations summarized within the box beneath it. To further assist with the interpretation of the results, the key parameters (maximum, minimum, and mean crack spacing and crack width) are summarized in Tables 5 and 6, respectively.

TABLE 5 Summary of critical statistics for monotonic crack spacing.

Load (kN)	Mean (mm)	Median (mm)	Maximum (mm)	Minimum (mm)
20	182.3	166.0	391.5	42.0
30	128.1	120.0	388.0	22.0
40	82.6	65.0	302.0	14.0
50	62.0	52.0	243.0	3.0
60	51.5	44.5	243.0	1.0
70	49.1	41.0	182.0	1.0
80	46.1	38.5	182.0	1.0
90	45.6	38.0	182.0	1.0

TABLE 6 Summary of critical statistics for crack width.

Load (kN)	Mean (mm)	Median (mm)	Maximum (mm)	Minimum (mm)
20	0.016	0.019	0.030	0.014
30	0.029	0.027	0.062	0.001
40	0.036	0.032	0.125	0.005
50	0.041	0.033	0.154	0.001
60	0.044	0.037	0.197	0.001
70	0.047	0.038	0.146	0.001
80	0.050	0.038	0.185	0.001
90	0.062	0.041	0.275	0.001

Examining all of the monotonic results in Figure 12, it can be observed that, as expected, the maximum and mean crack-width increases with increasing load, while the minimum crack-width remains relatively constant and close to zero. It is also observed that the interquartile range of the crack-widths increases, but the median crack-width remains relatively constant; this aligns with what is suggested by partial-interaction mechanics in that the formation and widening of secondary and tertiary cracks are associated with the stabilization or partial closure of primary cracks as a redistribution of stress between the reinforcement and concrete occurs.[53,54]

This behavior is expected in concrete with fibers because once cracks have localized (i.e., with a concrete strain of 0.0025 in Figure 5c), the stress transferred across the crack reduces with increases in crack-width, that is, the descending branch of the monotonic stress crack width relationship is followed. Hence as the total force in the prism increases, a larger proportion of this total force will need to be carried by the reinforcement, and an increase in reinforcement force can only be achieved through increased slip between the reinforcement and the concrete. Conversely, when the concrete only has microcracks, the concrete experiences strain hardening (Figure 5b), such that as the total prism force increases, the proportion taken by the concrete does not need to reduce, and as such, the increase in crack width remains small.

3.3.2 | Cyclic loading

The crack-width readings for the high-cycle fatigue tests are shown in Figure 13. The two green boxplots represent the crack-width data obtained at the trough and peak of the load cycles. The red box plots represent both the data obtained from monotonic loading before cycling and when loading to fail after cyclic loading (specimens C1–C3 only because the remainder of the specimens failed during load cycles). To allow for easy comparison to the monotonic load crack width behavior, the results obtained under monotonic loading are also presented using the purple boxplots.

Firstly, consider the readings taken at the peak and trough of each cycle (green boxes in Figure 13). It can be seen by comparing to the corresponding results obtained under monotonic loading (purple boxes) that the action of high-cycle fatigue has, in general, led to an increase in the maximum, mean and median crack widths, along with an increase in the interquartile range. Depending on the magnitude of the cyclic range, the increase in crack width can be up to 227%.

Now consider the behavior of the tests that were loaded to failure after a period of cyclic loading, that is the results in Figure 13a–c. By comparing the red boxes (loading to failure after cycling) with the purple boxes (monotonic loading only), even when the high-cycle fatigue is insufficient to fail the specimen, there is a

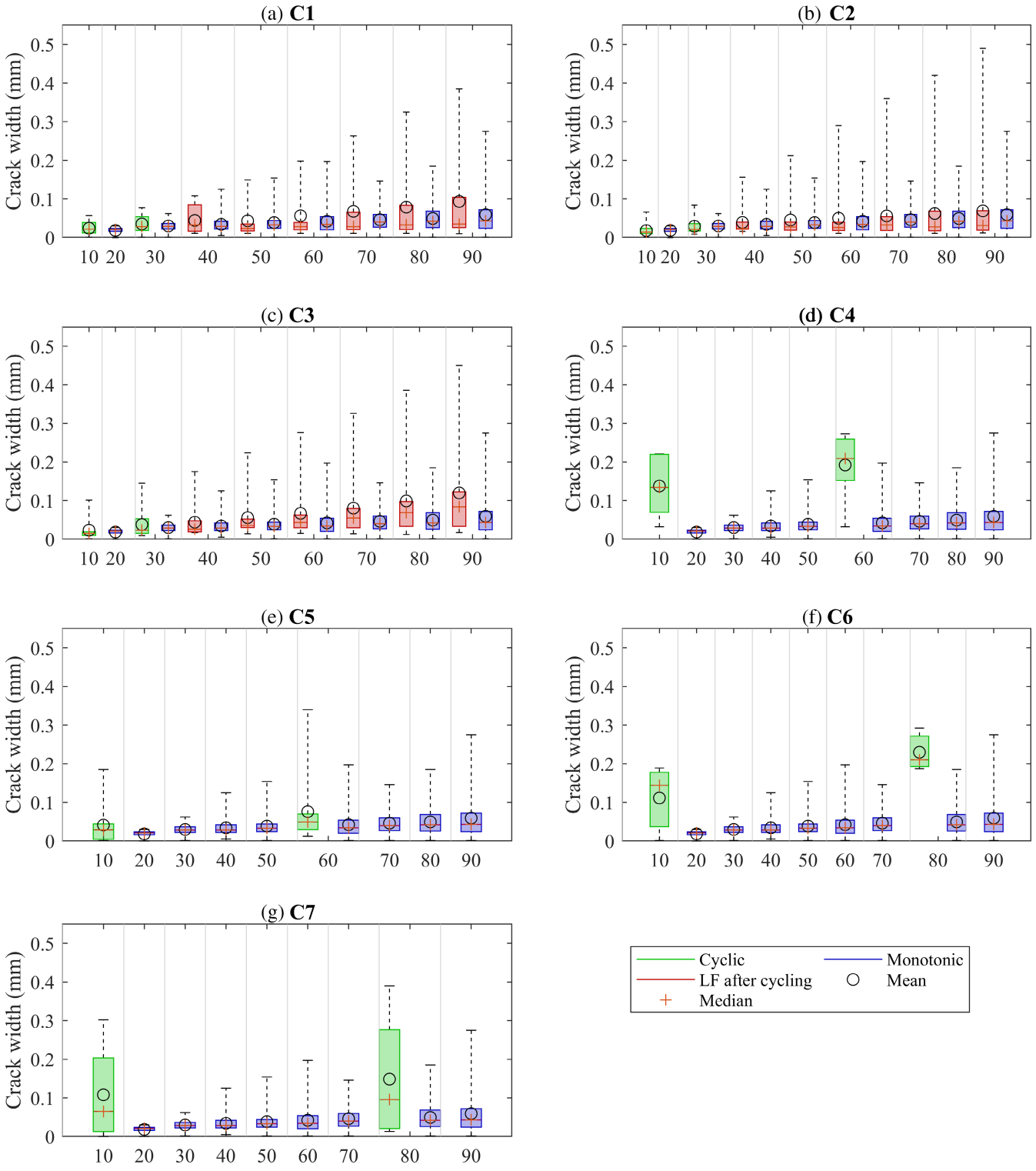

FIGURE 13 Crack widening per load step for cycled specimens and monotonic loading stage.

significant increase in the size of the cracks, and in particular the size of the largest crack.

In Figure 14, the crack width that was measured continuously by the LVDTs placed across the primary cracks is shown. The asterisks shown at the beginning of each curve identify the initial crack width. Taking Figure 14b as an example, where there are three cracks in specimen C2, named CwN-1, CwN-2 and CwS-1. The initials 'Cw' stands for crack width, the letter 'S' or 'N' locate the crack position as south or north, and the number refers to the crack number as given in Appendix S1, Figure S4. For the crack CwN-2, in Figure 14b, the initial crack is at

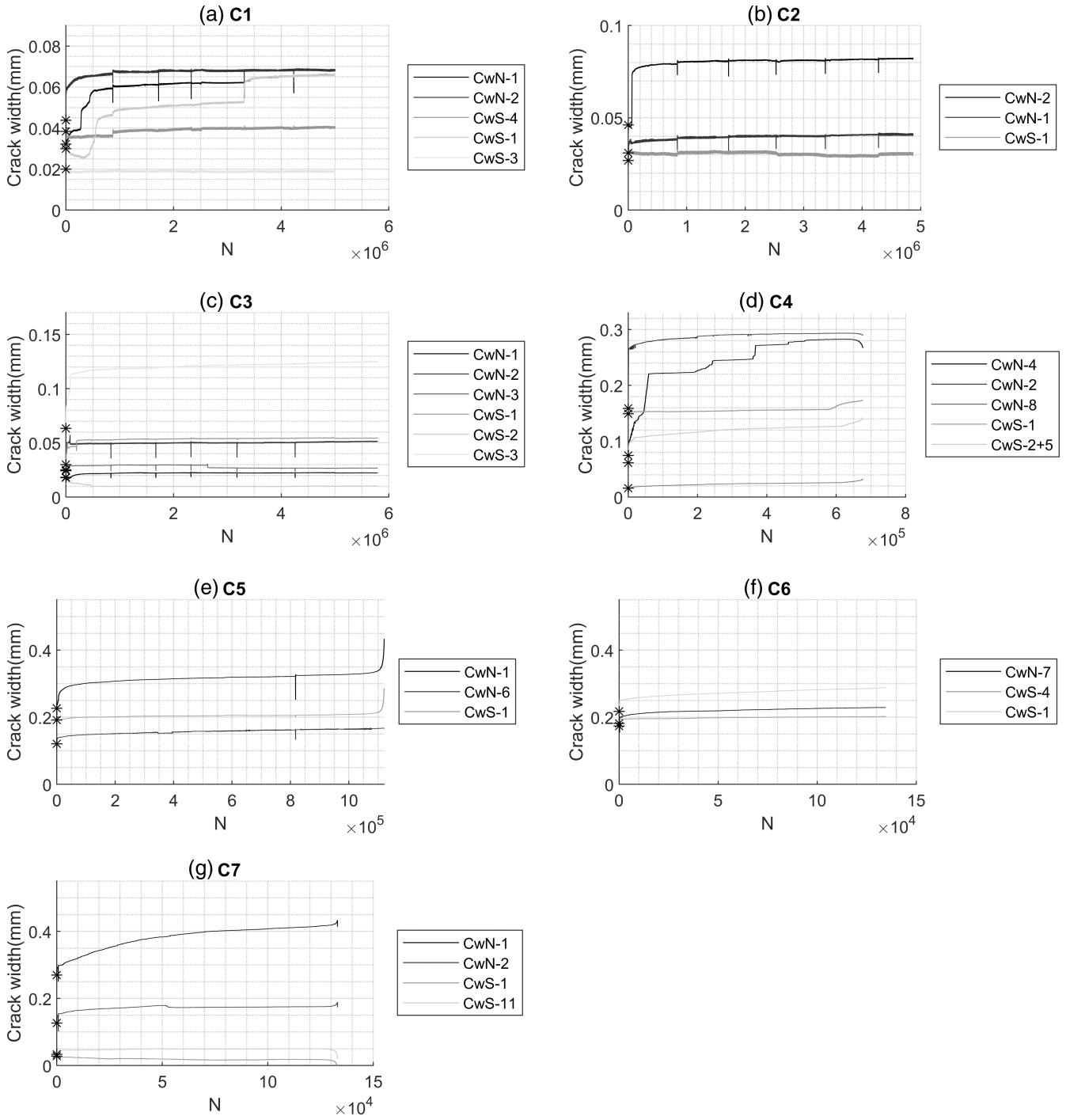

FIGURE 14 Crack widening during ciclic loading.

0.046 mm where the asterisks sit. During loading, it increases at a rapid rate before stabilizing. For specimens C4–C7, which failed during fatigue loading, a third component is observed during which the crack width rapidly increases immediately prior to failure.

Significantly, it can be observed that in all tests, regardless of cyclic range, or the number of cycles to failure, there is a significant difference in the width of the initial cracks. This variation in crack width can be explained by both the local variation in material properties, particularly the distribution of fibers, and the large variation in crack spacing.[55] The influence of the random nature of crack spacing is significant because, as shown in Table 7, the maximum crack spacing varied from 47 to 197 mm and the minimum crack spacing varied from 17 to 141 mm.

TABLE 7 Crack spacing for cracks measured with transducers.

Specimen	Crack	Maximum crack space (mm)	Minimum crack space (mm)
C1	CwN-1	78	73
	CwN-2	206	85
	CwS-4	120	19
	CwS-1	137	77
	CwS-3	137	57.5
C2	CwN-1	166	141
	CwN-2	141	91
	CwS-1	197	103
C3	CwN-1	63	52
	CwN-2	130	52
	CwN-3	138	130
	CwS-1	118	67
	CwS-2	97	55
	CwS-3	97	48
C4	CwN-2	50	22
	CwN-4	56	42
	CwN-8	119	57
	CwS-1	96.5	69.5
	CwS-2	96.5	22
	CwS-5	90	22
C5	CwN-1	102	33
	CwN-6	102	80
	CwS-1	71	63
C6	CwN-7	65	61
	CwS-4	124	66
	CwS-1	47	39
C7	CwN-1	67	17
	CwN-2	92	64
	CwS-1	79	30
	CwS-11	87	33

4 | PARTIAL-INTERACTION UNDER CYCLIC LOADING

The application of partial-interaction mechanics to simulate the formation of cracks, tension-stiffening and crack widening, including the impacts of fiber reinforcement and time-effects, is well established under monotonic loading, and both numerical and analytical solutions are widely available (e.g., Refs. 53,54,56,57). When considering cyclic loading, the same fundamental partial-interaction mechanics has been applied numerically to predict instantaneous behavior under a small number of large load cycles,[28,29] but application to high-cycle fatigue has not been considered. This is an expected outcome because the numerical partial-interaction analysis can be computationally expensive when considering cyclic loading, and simulation would likely be more time-consuming than physical testing. Given the complexity of directly applying detailed PI mechanics to each load cycle, here a simplified approach is proposed, and the reader is referred to articles on the detailed development under monotonic loading[1,54,58,59] and cyclic loading[28,29] for further details.

4.1 | Simplified PI model for high-cycle fatigue

The partial-interaction mechanism under cyclic loading can be simulated by allowing for the impact of load cycles on the reinforcement stress–strain behavior, the concrete stress–strain and stress crack width behavior (Figure 15a) and the bond between the reinforcement and the concrete (Figure 15b). These material properties have been quantified via material testing.[18,19]

The simplified model is then developed by only considering that we are only interested in the peak point of each cycle. This simplifies the analysis as it can be observed if every cycle has the same amplitude the slip will increase monotonically. Hence, the bond stress–slip relationship is always on the monotonic envelope, which is offset from the origin by some incremental slip (Figure 15c), and where this assumption can be made because at the peak of each cycle the crack width increases. When considering the behavior of a cracked tension stiffening prism, where again it is assumed that the crack width is increasing at the peak of each cycle, it can be assumed that the stress/crack width behavior follows the descending branch of the monotonic envelope in Figure 15a. Making the assumptions that the uncracked concrete and steel elastic modulus remain unaffected by high cycle fatigue at low cyclic ranges, a simplified modeling approach is proposed here to obtain the slip at the peak of a cycle. This simplified approach is considered to be important because of its low computational effort and because it allows for the calculation of the maximum average strains and crack widths within a given cycle, as these values control design.

In the simplified procedure, a monotonic analysis following the standard partial-interaction procedure outlined in Visintin et al.[28] is first applied to determine the distributions of slip and bond stress at the peak loading of the first cycle. From these results the range of shear stresses $R_\tau(x)$ along the length of the prism can then be estimated as

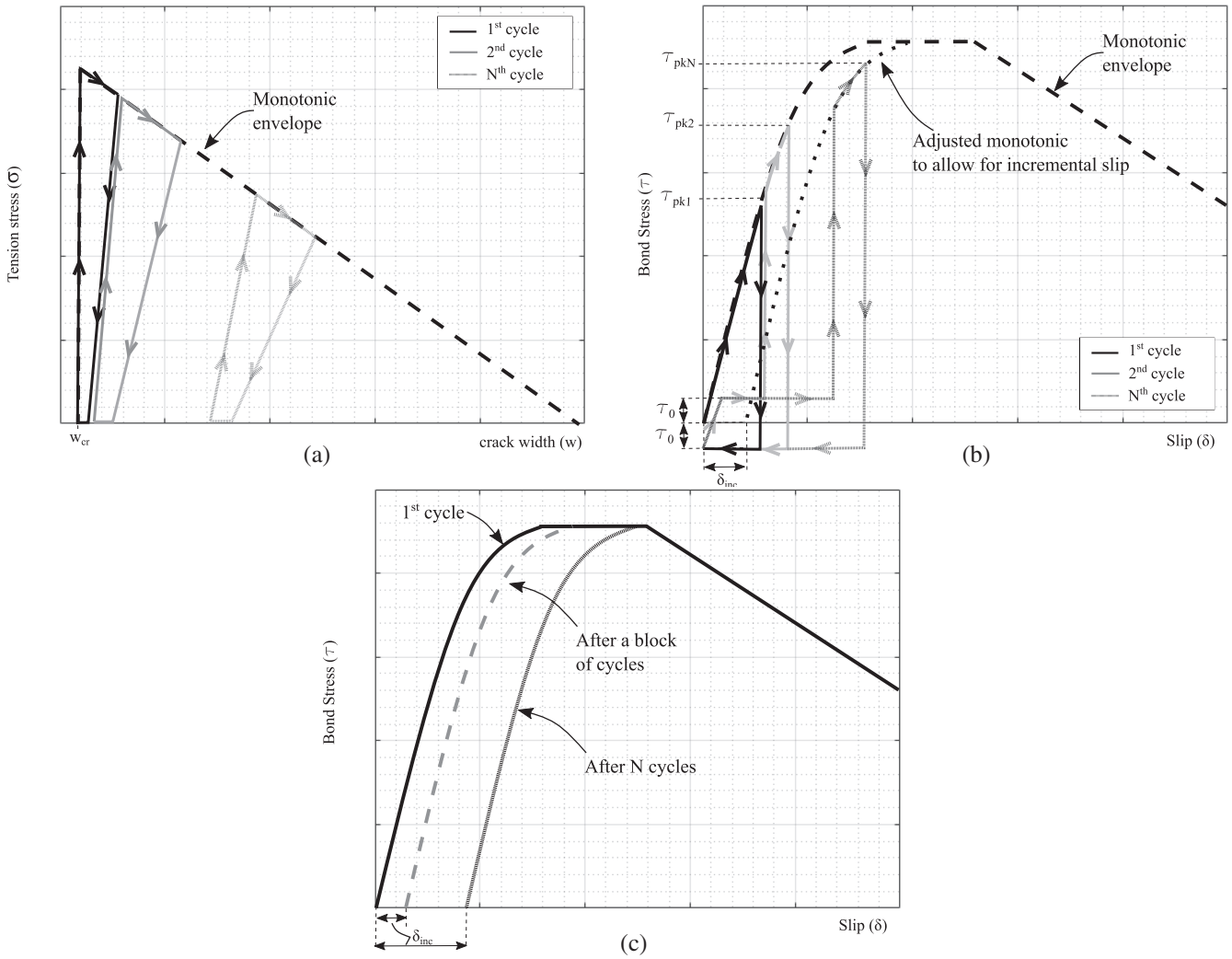

FIGURE 15 (a) Tensile–stress crack with model for UHPFRC; (b) bond fatigue model for reinforcement and UHPFRC; (c) bond model for application in PI numerical simulation.

$$R_{\tau(x)} = \frac{\tau_{\mathrm{pk}} - \tau_0}{\tau_{\max}} \tag{2}$$

where $\tau_{\max}$ is the bond strength, τ_{pk} is the bond stress at the peak of the cycle, and τ_0 is the bond stress at the trough of the cycle. This is then used to update the incremental slip for the bond stress–slip relationship. The partial interaction analysis is then repeated for the next cycle using the updated bond stress–slip relationship which is then used to update $R_r(x)$ and to compute the incremental slip accrued on this cycle. This is continued until the desired number of cycles is completed. This procedure is summarized in Figure 15b. Note that

$$\beta = L_{\mathrm{per}}\left(\frac{1}{E_{\mathrm{r}}A_{\mathrm{r}}} + \frac{1}{E_{\mathrm{c}}A_{\mathrm{c}}}\right) \tag{3}$$

where L_{per} is the bonded perimeter of the reinforcement in the tension chord, E_{r} is the elastic modulus of the reinforcement and E_{c} is the elastic modulus of the concrete. A_{r} is the cross-sectional area of the reinforcement and A_{c} is the cross-sectional area of the concrete.

To evaluate the crack spacing the closed form solution in Sturm[59] is recommended. To evaluate the bond stresses the bond stress slip model from Sepulveda et al.[19] is also recommended. In this model the monotonic part of the curve as shown in Figure 15c can be written in the form

$$\tau = \frac{\tau_{\max}}{\delta_1^{\alpha}}(\delta - \delta_{\mathrm{inc}})^{\alpha} \tag{4}$$

where δ_1 is the slip at the peak bond stress before cyclic loading, α is the non-linearity of the bond stress/slip relationship and δ_{inc} is the incremental slip accrued on the previous cycles. From Sepulveda et al.[19] the change in incremental slip for each cycle is given by

$$\Delta\delta_{inc} = A_1 R_\tau^{A_2} \quad (5)$$

where A_1 and A_2 are empirical coefficients derived from cyclic bond stress/slip tests.

Another interesting finding was that it was found to be unnecessary to calculate R_τ and to update the incremental slip on every cycle. Instead since R_τ does not change much cycle to cycle, a block of cycles can instead be applied which improves the computational efficiency of the model. So, a block of N cycles is then applied and based on the range $R_\tau(x)$ determined using Equation (2) and the number of cycles N, the corresponding bond stress for the next block of cycles can be determined using the bond properties in Figure 15c and Equation (4). Note if using blocks of cycles multiply the change in incremental slip in Equation (4) by the number of cycles in the block. The monotonic analysis is then repeated to obtain the shear stress at the peak of the Nth load cycle, which can be substituted in Equation (2) to obtain the cyclic range to be applied for the next block of N cycles.

To validate this approach, the experimentally measured average strain and crack width were simulated and the results of the comparison are shown in Figures 16 and 17, respectively. In applying the approach, the bond stress slip relationship was taken to be that quantified by Ref. 19 for the same concrete mix design, and τ_0 in Equation (2) was taken as zero because Sepulveda et al.[19] model was developed from tests conducted under load control and therefore does not include the negative shear stresses that can form as the slip reduces close to zero. Importantly, at the crack face, the concrete stresses fall

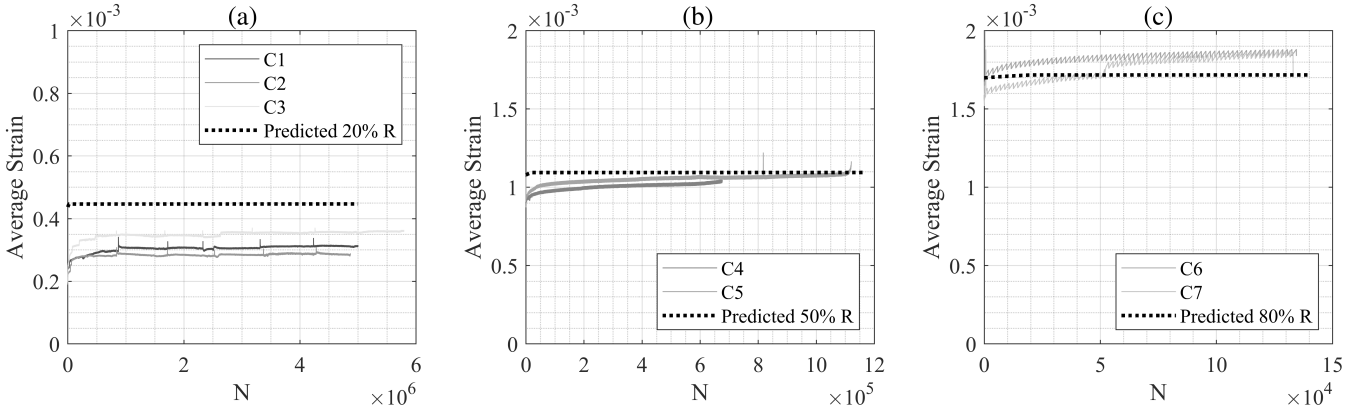

FIGURE 16 Model validation for the strain evolution during cyclic loading: (a) 20% range, (b) 50% range and (c) 80% range.

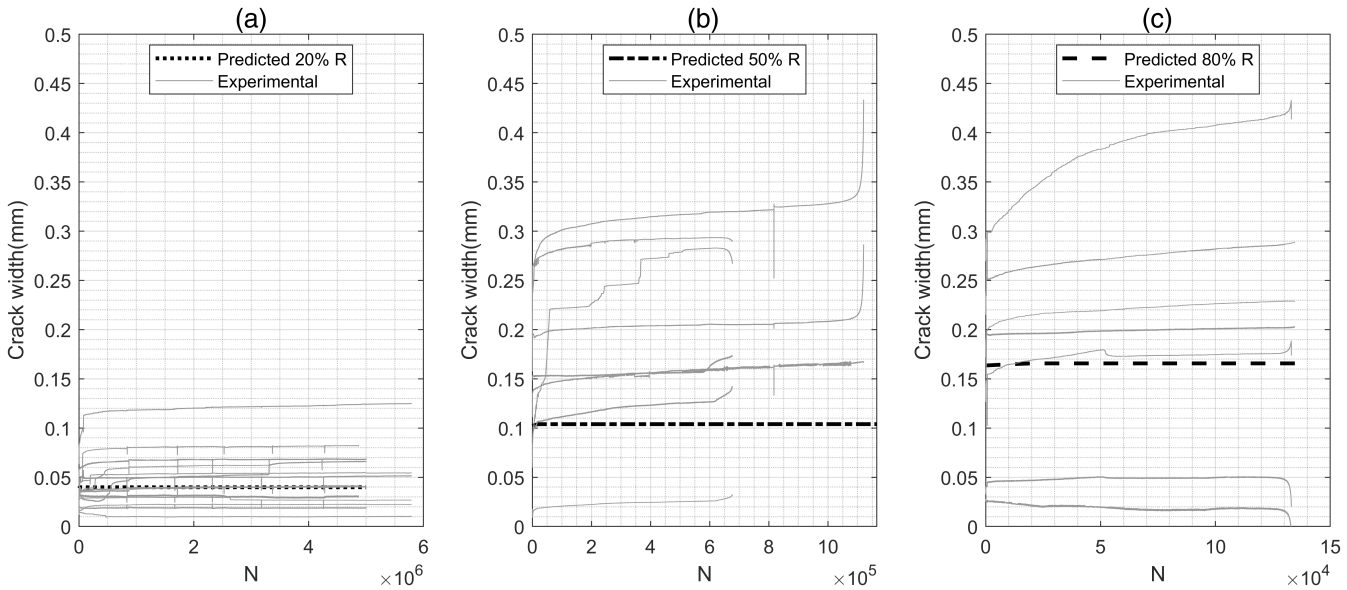

FIGURE 17 Model validation for the crack-width evolution during cyclic loading.

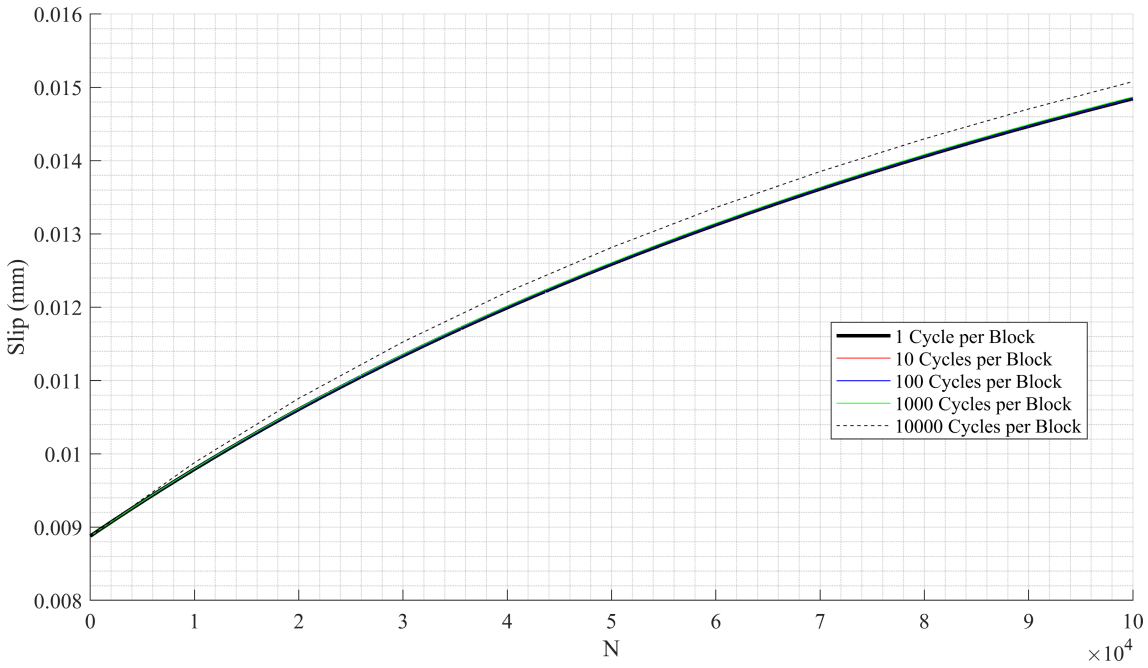

FIGURE 18 Sensitivity to blocks per cycle.

on the descending branch of the stress crack width relationship i.e. they follow the monotonic backbone curve as defined in Sepulveda et al.[18] for the same concrete as was used in these tension-stiffening tests.

For the analysis in Figures 16 and 17, blocks of 1000 cycles were applied based on the sensitivity analysis presented in Figure 18. When comparing the predicted and experimental results in Figure 17, it can be observed that there is, in general, a good correlation for the larger cyclic ranges, but at low cyclic ranges the average strain is overpredicted. It is expected that this occurs because of the significant scatter in the experimental and predicted results of the bond stress model, and further research is required to refine this material model at low cyclic ranges, particularly with tests that are cycled to failure.

When considering the crack width, it can be observed that the modeled results generally lie close to the average experimental results, and a significant scatter is expected here due to the variation in crack spacing.

5 | CONCLUSION

Research on the application of UHPFRC has shown that it has significant potential to improve the serviceability limit state behavior of reinforced concrete members. While there has been an increasing number of studies that have examined behavior, including the impact of time-effects and sustained loading, to date, very little information is available on the impact of high-cycle fatigue. This is important because the presence of high-cycle fatigue may impact both tension-stiffening and crack widening and therefore limit the ability to utilize the full capacity of fiber reinforcement.

To address this gap, this paper presents the results of an experimental campaign with 9 UHPFRC tension stiffening specimens subjected to monotonic and cyclic loads of different ranges and peaks. The tension stiffening specimens were either cycled until fatigue failure occurred or a block of cycles were applied, and then the specimen was loaded until the reinforcement yielded. The average strain, crack widths and crack spacings were measured during testing.

The outcomes of this testing have shown that:

1. During high-cycle fatigue, the average strain is observed to rapidly increase over a small number of cycles before stabilizing. Provided that rupture of the reinforcing does not occur, changes in tension-stiffening are minor and if loading to failure following a period of cyclic loading, the monotonic backbone is followed.
2. Although tension-stiffening experiences little impact due to high-cycle fatigue, the crack-width is highly influenced. During a period of cyclic loading, the crack width is significantly larger than that which is observed under an equivalent monotonic load (monotonic load is the same as the cyclic peak). If loaded monotonically after a period of cyclic loading, the crack widths are also significantly larger than expected from only monotonic loading. This outcome can be expected to impact the serviceability design of structures subjected to fatigue.

Importantly during cyclic loading, the minimum crack width is not significantly impacted, but the maximum crack width is significantly increased.

A simplified partial-interaction approach has been proposed to simulate the behavior at a cyclic peak. This approach allows for the application of a block of cycles rather than needing to simulate each cycle individually. Although highly simplified, validation against the test specimens shows a reasonable fit, particularly given the simplifying assumptions, the uncertainty in material properties and the random nature of cracking.

ACKNOWLEDGMENTS

This material is based upon work supported by the Australian Research Council Discovery Project 190102650. Open access publishing facilitated by The University of Adelaide, as part of the Wiley - The University of Adelaide agreement via the Council of Australian University Librarians.

DATA AVAILABILITY STATEMENT

All data, models, and code generated or used during the study appear in the submitted article.

ORCID

P. Visintin https://orcid.org/0000-0002-4544-2043

REFERENCES

1. Visintin P, Oehlers DJ, Muhamad R, Wu C. Partial-interaction short term serviceability deflection of RC beams. Eng Struct. 2013;56:993–1006. https://doi.org/10.1016/j.engstruct.2013.06.021
2. Marti P, Alvarez M, Kaufmann W, Sigrist V. Tension chord model for structural concrete. Struct Eng Int. 1998;8:287–98. https://doi.org/10.2749/101686698780488875
3. Sturm AB, Visintin P, Oehlers DJ. Rational design approach for the instantaneous and time-dependent serviceability deflections and crack widths of FRC and UHPFRC continuous and simply supported beams. J Struct Eng. 2019;145:4019138. https://doi.org/10.1061/(asce)st.1943-541x.0002423
4. Higgins L, Forth JP, Neville A, Jones R, Hodgson T. Behaviour of cracked reinforced concrete beams under repeated and sustained load types. Eng Struct. 2013;56:457–65. https://doi.org/10.1016/j.engstruct.2013.05.034
5. Gilbert RI, Wu HQ. Time-dependent stiffness of cracked reinforced concrete elements under sustained actions. Aust J Struct Eng. 2009;9:151–8. https://doi.org/10.1080/13287982.2009.11465018
6. Amin A, Foster SJ, Kaufmann W. Instantaneous deflection calculation for steel fibre reinforced concrete one way members. Eng Struct. 2017;131:438–45. https://doi.org/10.1016/J.ENGSTRUCT.2016.10.041
7. Mitchell D, Abrishami HH. Influence of steel fibres on tension stiffening. ACI Struct J. 1997;94:769–73.
8. Bischoff PH. Reevaluation of deflection prediction for concrete beams reinforced with steel and fiber reinforced polymer bars. J Struct Eng. 2005;131:752–67. https://doi.org/10.1061/(ASCE)0733-9445(2005)131:5(752)
9. Zanuy C, Albajar L, de la Fuente P. On the cracking behaviour of the reinforced concrete tension chord under repeated loading. Mater Struct. 2010;43:611–32. https://doi.org/10.1617/s11527-009-9516-9
10. Villafán TA. Fatigue of the tension-stiffening effect in reinforced concrete. Hamburg: Technischen Universität Hamburg; 2021. https://tore.tuhh.de/handle/11420/9744
11. Standards Australia, Concrete structures (AS 3600:2018). Sydney: Standards Australia; 2018.
12. CEB-Fib, Model Code 2010. Lausanne: International Federation for Structural Concrete (fib); 2010. https://doi.org/10.1007/s13398-014-0173-7.2.
13. CEB-Fib. State-of-art report: constitutive modelling of high strength/high performance concrete - Bulletin 42. 2008.
14. Thun H, Ohlsson U, Elfgren L. A deformation criterion for fatigue of concrete in tension. Struct Concr. 2011;12:187–97. https://doi.org/10.1002/suco.201100013
15. Koch R, Balázs GL. Slip increase under cyclic and long term loads. Otto-Graf J Res Test Mater Res Test Mater. 1993;4:160–91.
16. Rehm G, Eligehausen R. Bond of ribbed bars under high cycle repeated loads. ACI J. 1979;76:297–309.
17. Oh BH, Kim SH. Realistic models for local bond stress-slip of reinforced concrete under repeated loading. J Struct Eng. 2007;133:216–24. https://doi.org/10.1061/(asce)0733-9445(2007)133:2(216)
18. Sepulveda BDG, Visintin P, Oehlers DJ. Quantifying the fatigue material properties of UHPFRC with steel microfibers at cracks. J Struct Eng. 2021;147:1–17. https://doi.org/10.1061/(asce)st.1943-541x.0003051
19. Sepulveda BDG, Visintin P, Oehlers DJ. Fatigue bond-slip properties of steel reinforcing bars embedded in UHPFRC: extraction and development of an accumulated damage law. Case Stud Constr Mater. 2022;17:e01370. https://doi.org/10.1016/j.cscm.2022.e01370
20. Isojeh B, El-Zeghayar M, Vecchio FJ. Fatigue behavior of steel fiber concrete in direct tension. J Mater Civ Eng. 2017;29:4017130-1–9. https://doi.org/10.1061/(ASCE)MT.1943-5533.0001949
21. Zhang J, Stang H, Li VC. Experimental study on crack bridging in FRC under uniaxial fatigue tension. J Mater Civ Eng. 2000;12:66–73.
22. Rocha M, Brühwiler E, Nussbaumer A. Fatigue behaviour prediction of steel reinforcement bars using an adapted Navarro and de Los Rios model. Int J Fatigue. 2015;75:198–204. https://doi.org/10.1016/j.ijfatigue.2015.01.015
23. Tilly GP. Fatigue testing and performance of steel reinforcement bars. Matériaux Constr. 1984;17:43–9. https://doi.org/10.1007/BF02474055
24. Bresler B, Betero V. Behaviour of reinforced concrete under repeated load. J Struct Div. 1968;94:1567–90.
25. Fantilli AP, Vallini P. Strains in steel bars of reinforced concrete elements subjected to repeated loads. J Strain Anal Eng Des. 2004;39:447–57. https://doi.org/10.1243/0309324041896489
26. Tassios TP, Yannopoutos PJ. Analytical studies on reinforced concrete members under cyclic loading based on bond stress-slip relationships. ACI J Proc. 1981;78:206–16. https://doi.org/10.14359/6919
27. Zanuy C, de la Fuente P, Albajar L. Estimation of parameters defining negative tension stiffening. Eng Struct. 2010;32:3355–62. https://doi.org/10.1016/J.ENGSTRUCT.2010.07.009

28. Visintin P, Oehlers DJ, Wu C, Griffit MC. The reinforcement contribution to the cyclic behaviour of reinforced concrete beam hinges. Earthq Eng Struct Dyn. 2012;41:1591–608. https://doi.org/10.1002/eqe.1189
29. Shukri AA, Visintin P, Oehlers DJ, Jumaat MZ. Mechanics model for simulating RC hinges under reversed cyclic loading. Materials (Basel). 2016;9:305. https://doi.org/10.3390/ma9040305
30. Azmee NM, Shafiq N. Ultra-high performance concrete: from fundamental to applications. Case Stud Constr Mater. 2018;9:1–15. https://doi.org/10.1016/J.CSCM.2018.E00197
31. Zhong R, Wille K, Viegas R. Material efficiency in the design of UHPC paste from a life cycle point of view. Construct Build Mater. 2018;160:505–13. https://doi.org/10.1016/j.conbuildmat.2017.11.049
32. Abbas S, Nehdi ML, Saleem MA. Ultra-high performance concrete: mechanical performance, durability, sustainability and implementation challenges. Int J Concr Struct Mater. 2016;10:271–95. https://doi.org/10.1007/s40069-016-0157-4
33. Hajar Z, Resplendino J, Lecointre D, Petitjean J, Simon A. Ultra-high-performance concretes: first recommendations and examples of application. 2004.
34. Dong S, Wang Y, Ashour A, Han B, Ou J. Uniaxial compressive fatigue behavior of ultra-high performance concrete reinforced with super-fine stainless wires. Int J Fatigue. 2021;142:105959. https://doi.org/10.1016/j.ijfatigue.2020.105959
35. Li L, Xu L, Huang L, Xu F, Huang Y, Cui K, et al. Compressive fatigue behaviors of ultra-high performance concrete containing coarse aggregate. Cem Concr Compos. 2022;128:104425. https://doi.org/10.1016/j.cemconcomp.2022.104425
36. Basaldella M, Jentsch M, Oneschkow N, Markert M, Lohaus L. Compressive fatigue investigation on high-strength and ultra-high-strength concrete within the SPP 2020. Materials (Basel). 2022;15:3793. https://doi.org/10.3390/ma15113793
37. Makita T, Brühwiler E. Tensile fatigue behaviour of ultra-high performance fibre reinforced concrete (UHPFRC). Mater Struct. 2014;47:475–91. https://doi.org/10.1617/s11527-013-0073-x
38. Makita T, Brühwiler E. Tensile fatigue behaviour of ultra-high performance fibre reinforced concrete combined with steel rebars (R-UHPFRC). Int J Fatigue. 2014;59:145–52. https://doi.org/10.1016/J.IJFATIGUE.2013.09.004
39. Koschemann M, Kuhn T, Speck K, Curbach M. Bond behaviour of reinforced concrete under high cycle fatigue pull-out loading, in: better, smarter, stronger proc. Fib Congr. 2018;2018.
40. Behloul M, Chanvillard G, Pimienta P, Pineaud A, Rivillon P. Fatigue flexural behavior of pre-cracked specimens of special UHPFRC. 2005;228:1253–68.
41. Parant E, Rossi P, Boulay C. Fatigue behavior of a multi-scale cement composite. Cem Concr Res. 2007;37:264–9. https://doi.org/10.1016/j.cemconres.2006.04.006
42. Rossi P, Parant E. Damage mechanisms analysis of a multi-scale fibre reinforced cement-based composite subjected to impact and fatigue loading conditions. Cem Concr Res. 2008;38:413–21. https://doi.org/10.1016/j.cemconres.2007.09.002
43. Al-Azzawi BS, Karihaloo BL. Flexural fatigue behavior of a self-compacting ultrahigh performance fiber-reinforced concrete. J Mater Civ Eng. 2017;29:1–9. https://doi.org/10.1061/(asce)mt.1943-5533.0002051
44. Carlesso DM, de la Fuente A, Cavalaro SHP. Fatigue of cracked high performance fiber reinforced concrete subjected to bending. Construct Build Mater. 2019;220:444–55. https://doi.org/10.1016/J.CONBUILDMAT.2019.06.038
45. Niu Y, Huang H, Wei J, Jiao C, Miao Q. Investigation of fatigue crack propagation behavior in steel fiber-reinforced ultra-high-performance concrete (UHPC) under cyclic flexural loading. Compos Struct. 2022;282:115126. https://doi.org/10.1016/j.compstruct.2021.115126
46. Sawicki B, Brühwiler E. Fatigue resistance of reinforced UHPFRC beams. Int J Fatigue. 2021;148:106216. https://doi.org/10.1016/j.ijfatigue.2021.106216
47. Visintin P, Sturm AB, Mohamed Ali MS, Oehlers DJ. Blending macro- and micro-fibres to enhance the serviceability behaviour of UHPFRC. Aust J Civ Eng. 2018;16:106–21. https://doi.org/10.1080/14488353.2018.1463608
48. Australian Standard. Methods of testing concrete method 17: determination of the static chord modulus of elasticity and Poisson's ratio of concrete specimens (AS 1012.17-1997). Sydney: Standards Australia; 1997. p. 1–16.
49. ASTM:C157/C157M-08. Standard test method for length change of hardened hydraulic-cement mortar and concrete. ASTM Int. 2008;8:1–7. https://doi.org/10.1520/C0157_C0157M-17
50. I.O. for Standardization. Metallic materials - Tensile testing - Part 1: Method of test at room temperature (ISO 6892-1:2019). 2019.
51. Australian Standard, General purpose and blended cements (AS 3972:2010). Sydney: Standards Australia; 2010.
52. Standards Australia/Standards New Zealand. Supplementary cementitious materials, Part 3: Amorphous silica (AS/NZS 3582.3:2016). 2016.
53. Muhamad R, Mohamed Ali MS, Oehlers DJ, Griffith M. The tension stiffening mechanism in reinforced concrete prisms. Adv Struct Eng. 2012;15:2053–69. https://doi.org/10.1260/1369-4332.15.12.2053
54. Sturm AB, Visintin P, Oehlers DJ. Time-dependent serviceability behavior of reinforced concrete beams: partial interaction tension stiffening mechanics. Int Fed Struct Concr. 2018;19:508–23. https://doi.org/10.1002/suco.201700021
55. Sturm AB, Visintin P, Bennett B. A hybrid deterministic-probabilistic approach for the characteristic crack widths and crack spacings in reinforced concrete tension and flexural members. Eng Struct. 2022;256:114071. https://doi.org/10.1016/j.engstruct.2022.114071
56. Visintin P, Oehlers DJ. Fundamental mechanics that govern the flexural behaviour of reinforced concrete beams with fibre-reinforced concrete. Adv Struct Eng. 2018;21:1088–102. https://doi.org/10.1177/1369433217739705
57. Zhang T, Visintin P, Oehlers DJ. Partial-interaction tension-stiffening properties for numerical simulations. Adv Struct Eng. 2017;20:812–21. https://doi.org/10.1177/1369433216660654
58. Oehlers DJ, Mohamed Ali MS, Haskett M, Lucas W, Muhamad R, Visintin P. FRP-reinforced concrete beams: unified approach based on IC theory. J Compos Constr. 2011;15:293–303. https://doi.org/10.1061/(ASCE)CC.1943-5614.0000173
59. Sturm AB, Visintin P, Oehlers DJ, Seracino R. Time-dependent tension-stiffening mechanics of fiber-reinforced and ultra-high-performance fiber-reinforced concrete. J Struct Eng. 2018;144:4018122. https://doi.org/10.1061/(asce)st.1943-541x.0002107

AUTHOR BIOGRAPHIES

B. D. G. Sepulveda, School of Civil, Environmental and Mining Engineering, The University of Adelaide, Adelaide, South Australia 5005, Australia. Email: barbara.giorginisepulveda@adelaide.edu.au.

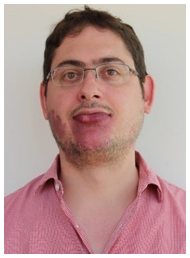

P. Visintin, School of Civil, Environmental and Mining Engineering, The University of Adelaide, Adelaide, South Australia 5005, Australia. Email: phillip.visintin@adelaide.edu.au.

A. B. Sturm, National Cheng Kung University, Tainan, Taiwan. Email: 11010067@gs.ncku.edu.tw.

D. J. Oehlers, School of Civil, Environmental and Mining Engineering, The University of Adelaide, Adelaide, South Australia 5005, Australia. Email: deric.oehlers@adelaide.edu.au.

SUPPORTING INFORMATION

Additional supporting information can be found online in the Supporting Information section at the end of this article.

How to cite this article: Sepulveda BDG, Visintin P, Sturm AB, Oehlers DJ. Experimental and theoretical analysis of cracking and tension stiffening in UHPFRC under high-cycle fatigue. Structural Concrete. 2024;25(1):379–402. https://doi.org/10.1002/suco.202200815